



Hallucination Reduction with CASAL: Contrastive Activation Steering for Amortized Learning

Wannan (Winnie) Yang^{*†}

Xinchi Qiu

Lei (Jade) Yu

Yuchen Zhang

Oliver Aobo Yang

Narine Kokhlikyan

Nicola Cancedda

Diego Garcia-Olano

Meta Superintelligence Labs

Abstract

Large Language Models (LLMs) exhibit impressive capabilities but often hallucinate, confidently providing incorrect answers instead of admitting ignorance. Prior work has shown that models encode linear representations of their own knowledge and that activation steering can reduce hallucinations. These approaches, however, require real-time monitoring and intervention during inference. We introduce **Contrastive Activation Steering for Amortized Learning (CASAL)**, an efficient algorithm that connects interpretability with amortized optimization. CASAL directly bakes the benefits of activation steering into model’s weights. Once trained, LLMs answer questions they know while abstaining from answering those they do not. CASAL’s light-weight design requires training only a submodule of a single transformer layer and yet reduces hallucination by $\sim 30\%$ - 40% across multiple short-form QA benchmarks. CASAL is $\sim 30\times$ more compute-efficient and $\sim 20\times$ more data-efficient than strong LoRA-based baselines such as SFT and DPO, boosting its practical applicability in data scarce domains. Importantly, CASAL also generalizes effectively to out-of-distribution (OOD) domains. We showcase CASAL’s flexibility in mitigating hallucinations in both text-only and vision-language models. To our knowledge, CASAL is the first steering-based training method that has been shown to be effective for both dense and Mixture-of-Experts (MoE) models. CASAL represents a promising step forward for applying interpretability-inspired method for practical deployment in production systems.

1 Introduction

Large Language Models (LLMs) have demonstrated near-human or even superhuman intellectual capabilities (Brown et al., 2020; Ouyang et al., 2022; OpenAI et al., 2024). Yet despite these successes, they sometimes fail in striking ways. A central failure mode is hallucination: the tendency to confidently generate false or unsupported information. Hallucinations undermine trust and restrict the safe deployment of LLMs in real-world settings where factual reliability is critical (Rawte et al., 2023; Gekhman et al., 2024a; Shen et al., 2025a).

^{*}Work done at Meta

[†]Corresponding author: winnieyangwn96@gmail.com

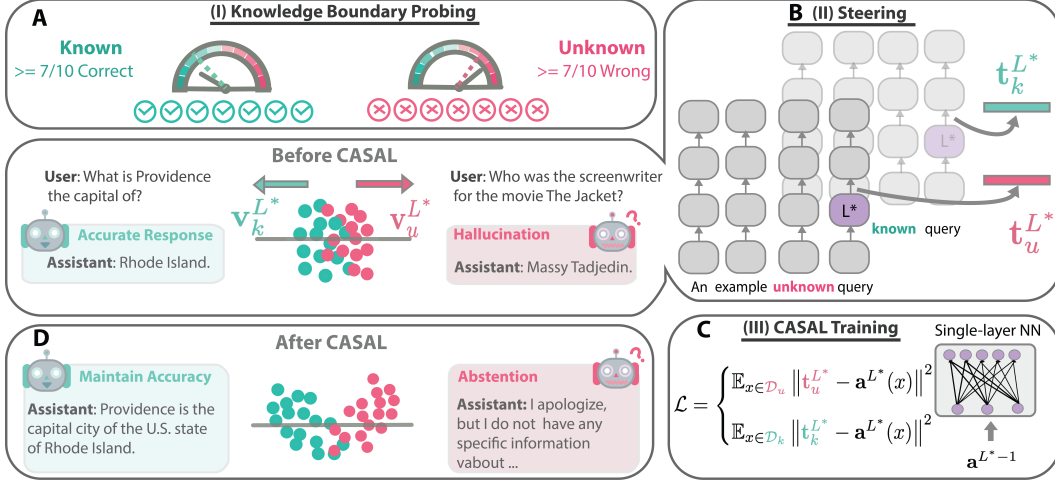


Figure 1: **Overview of the CASAL algorithm.** (A) **Knowledge Probing:** CASAL starts by probing the model to figure out what it knows vs doesn't know. Multiple responses per query are sampled to classify queries as **known** (\mathcal{D}_k) or **unknown** (\mathcal{D}_u). (B) **Steering:** Difference in means are computed to construct steering vectors (v_u^{L*} and v_k^{L*}). Target activations (t_u^{L*} and t_k^{L*}) are obtained by adding these steering vectors to the residual stream activation. **Pre-CASAL Behavior:** Prior to training, the model often hallucinates and produces incorrect answers for **unknown** queries. (C) **CASAL Training:** CASAL training is essentially "amortized activation steering", where instead of repeatedly steering activations online, we train a small subnetwork (a single layer NN) to approximate the steering solution offline. (D) **Post-CASAL Activations and Behavior:** After training, the model learns a sharper representation with a clearer knowledge boundary. It maintains correct answers on **known** queries while abstaining from answering **unknown** ones.

Recent interpretability studies—using sparse autoencoder (SAE) features (Templeton et al., 2024) or residual stream activations (Rimsky et al., 2024; Turner et al., 2024)—have revealed that LLMs encode a form of self-knowledge. Specifically, the activations associated with known versus unknown knowledge can be separated along linear directions (Ji et al., 2025; Ferrando et al., 2025). Moreover, steering these representations reduces overconfidence and enables models to acknowledge uncertainty. However, prior work primarily focuses on inference-time interventions, leaving a significant gap in their practicality as part of scalable alignment pipelines.

If LLMs' internal states already reflect what is known versus unknown, why do they still produce confident but false answers instead of abstaining when uncertain? We hypothesize that a key cause lies in the training paradigm of LLMs (Li et al., 2025a; Kalai et al., 2025). During pretraining, the language modeling objective rewards predicting the next token, even under uncertainty, encouraging plausible continuations rather than expressions of ignorance. Reinforcement learning from human feedback (RLHF) amplifies this tendency: optimizing for "helpfulness" reinforces confident, fluent responses, even if they are fabricated (Gekhman et al., 2024b).

In this work, we propose an alternative training objective—one that leverages the model's own internal representations to align behavior with knowledge boundaries. Our core hypothesis is that if models are trained to directly utilize their own representations of known and unknown, their generations will better reflect what they truly "know". Concretely, we replace the standard cross-entropy loss with a local representation loss applied to residual stream activations. Whereas cross-entropy loss provides a learning signal from *external* supervision (the training corpus), representation loss provides a learning signal from *within*: the model's hidden activations.

Importantly, CASAL is among the first approaches to *rely solely on a representation-level objective* for training language models. Prior studies such as RepE (Zou et al., 2025), ReFAT (Yu et al., 2025), and others (Yu et al., 2024a; Casademunt et al., 2025; Chen et al., 2025b; Yousefpour et al., 2025) have explored representation-level fine-tuning, but all employed representation losses as auxiliary signals

alongside standard objectives. By contrast, **CASAL treats representation loss as the only and the primary optimization objective**, directly teaching the model to utilize its hidden representation.

Our approach connects insights from two fields: interpretability and amortized optimization. Amortized optimization (Kingma and Welling, 2013; Rezende et al., 2014; Gershman and Goodman, 2014) is a paradigm where costly repeated optimizations are replaced by training a parametric function that approximates the solution. CASAL instantiates this idea by incorporating activation steering into training: **we "amortize" the activation steering process by training a lightweight subnetwork** that learns to approximate the steering solution, embedding the knowledge boundary directly into the model’s weights.

We highlight our main contributions as:

- **Effective Algorithm:** Introducing a training method inspired by interpretability findings and amortized optimization. CASAL enables models to admit ignorance for unknown questions, reducing hallucination rates by $\sim 30\%$ - 40% across multiple short-form QA benchmarks.
- **Efficiency Gains:** CASAL’s objective function enables local and lightweight parameter updates, delivering $\sim 30\times$ **higher compute efficiency (FLOPs per token)** and requires $\sim 20\times$ **less training data** (with as little as ~ 640 training data) to achieve the same level of performance compared to LoRA-based SFT and DPO.
- **Robust Generalization:** The trained model retains its general capabilities while avoiding excessive refusals. At the same time, it successfully generalizes refusal behavior to unknown queries sampled from out-of-distribution (OOD) data.
- **Versatility:** CASAL training is modality-agnostic, effectively mitigating hallucination in both text-only and **multimodal models**.
- **Broad Applicability:** We present *the first* ever steering-based training framework with *general* applicability to both **dense and Mixture-of-Experts (MoE) models**.

2 CASAL

We now introduce our method, CASAL, which integrates insights from interpretability and amortized optimization to build a lightweight, efficient training framework. The full pipeline is shown in Figure 1, summarized in Algorithm 1. At a high level, CASAL can be understood as an instance of *amortized optimization*: instead of repeatedly solving the steering problem at inference time, we train a parametric subnetwork to approximate this solution once, thereby "amortizing" the resource use of activation steering across all future queries. This perspective motivates the name: **Contrastive Activation Steering for Amortized Learning (CASAL)**. CASAL proceeds in three stages:

2.1 STEP 1: Knowledge Boundary Probing

CASAL begins by probing the model to delineate its knowledge boundary. For each input $x \in \mathcal{D}$, we sample $k = 10$ completions and compare them to ground-truth answers. For each question, if at least τ generations are correct, x is labeled as **known**; if less than 3 generations are incorrect, it is labeled as **unknown**. This produces two subsets: \mathcal{D}_k and \mathcal{D}_u , which are later used for contrastive steering. We systematically evaluated different threshold values $\tau \in \{3, 4, 5, 6, 7, 8\}$ and found that hallucination reduction performance remains robust across this range (Appendix I). We adopt a relatively strict threshold of $\tau = 7$ to ensure high-confidence separation: the model abstains only on knowledge it does not possess, and responds only when it demonstrates consistent correctness. This choice reduces ambiguous cases near the decision boundary. Consistent with previous literature (Ferrando et al., 2025; Grattafiori et al., 2024), the knowledge probing step creates the known versus unknown labels subsequently used for steering our training baseline methods such as SFT and DPO, and therefore does not introduce additional computational cost specific to CASAL. We evaluate CASAL on three datasets—TriviaQA (Joshi et al., 2017b), PopQA (Mallen et al., 2023b), and EntityQA (Ferrando et al., 2025)—with dataset details provided in Appendix G.1.

Algorithm 1 CASAL: Contrastive Activation Steering for Amortized Learning

Require: Dataset \mathcal{D} ; frozen model M_{original} with l layers; target layer L^* ; weight of one sub-module of the original model $W_{\text{original}}^{L^*}$; residual activations $\mathbf{a}^{L^*}(x)$ at target layer; α as the strength for steering; a one-layer neural network (NN) M_{train} for fine-tuning; weights after training the model M_{train} with CASAL $W_{\text{trained}}^{L^*}$; epochs for training E .

STEP 1: Knowledge boundary probing **known / unknown**

- 1: Set $k = 10$, threshold $\tau = 7$
- 2: **for** $x \in \mathcal{D}$ **do**
- 3: Sample k responses $\{y^{(i)}(x)\}$; $s(x) = \sum_i \mathbf{1}[y^{(i)}(x) \text{ correct}]$
- 4: **if** $s(x) \geq \tau$ **then** $\mathcal{D}_k \leftarrow \mathcal{D}_k \cup \{x\}$ ▷ "known" set \mathcal{D}_k
- 5: **else if** $k - s(x) \geq \tau$ **then** $\mathcal{D}_u \leftarrow \mathcal{D}_u \cup \{x\}$ ▷ "unknown" set \mathcal{D}_u
- 6: **end if**
- 7: **end for**

STEP 2: Steering

- 8: $\bar{\mathbf{a}}_u^{L^*} = \frac{1}{|\mathcal{D}_u|} \sum_{x \in \mathcal{D}_u} \mathbf{a}^{L^*}(x)$, $\bar{\mathbf{a}}_k^{L^*} = \frac{1}{|\mathcal{D}_k|} \sum_{x \in \mathcal{D}_k} \mathbf{a}^{L^*}(x)$ ▷ mean activations
- 9: $\mathbf{v}_u^{L^*} = \bar{\mathbf{a}}_u^{L^*} - \bar{\mathbf{a}}_k^{L^*}$, $\mathbf{v}_k^{L^*} = \bar{\mathbf{a}}_k^{L^*} - \bar{\mathbf{a}}_u^{L^*}$ ▷ steering vectors
- 10: $\mathbf{t}_u^{L^*}(x) = \mathbf{a}^{L^*}(x) + \alpha \cdot \mathbf{v}_u^{L^*}$ for $x \in \mathcal{D}_u$ ▷ "abstain when you don't know"
- 11: $\mathbf{t}_k^{L^*}(x) = \mathbf{a}^{L^*}(x) + \alpha \cdot \mathbf{v}_k^{L^*}$ for $x \in \mathcal{D}_k$ ▷ "answer when you know"

STEP 3: CASAL training

- 12: Initialize M_{train} with $W_{\text{original}}^{L^*}$ ▷ one-layer fine-tuning
- 13: **for** $e = 1 \dots E$ **do**
- 14: $\mathcal{L}_u = \mathbb{E}_{x \in \mathcal{D}_u} \|\mathbf{t}_u^{L^*}(x) - \mathbf{a}^{L^*}(x)\|^2$ ▷ "unknown" loss
- 15: $\mathcal{L}_k = \mathbb{E}_{x \in \mathcal{D}_k} \|\mathbf{t}_k^{L^*}(x) - \mathbf{a}^{L^*}(x)\|^2$ ▷ "known" loss
- 16: $\mathcal{L} \leftarrow \mathcal{L}_u + \mathcal{L}_k$; update W^{L^*} by $\nabla \mathcal{L}$
- 17: **end for**
- 18: Substitute the weights from the original transformer model M_{original} with weights from the trained subnetwork M_{train} : $W_{\text{original}}^{L^*} \leftarrow W_{\text{trained}}^{L^*}$

Ensure: Loss \mathcal{L}

2.2 STEP 2: Steering

Next, CASAL constructs steering vectors to reshape internal representations. For each query x , we extract residual stream activations $\mathbf{a}^{L^*}(x)$ at a designated target layer L^* . We then compute mean activations for **known** and **unknown** subsets ($\bar{\mathbf{a}}_k^{L^*}$ and $\bar{\mathbf{a}}_u^{L^*}$) and construct steering vectors by taking difference in means, resulting in two vectors: $\mathbf{v}_u^{L^*}$ for abstaining when the model lacks knowledge, and $\mathbf{v}_k^{L^*}$ for reinforcing correct answering when the model does know. The steering vectors are then added to the residual stream activations, yielding target activations $\mathbf{t}_u^{L^*}$ and $\mathbf{t}_k^{L^*}$. Further details for steering and target layer selection procedures are included in Appendix C.

2.3 STEP 3: CASAL Training

Finally, CASAL trains a lightweight one-layer network M_{train} —initialized by copying the entire sub-module weight matrix $W_{\text{original}}^{L^*}$ from layer L^* of the original model—to align activations with their targets. Using a mean squared error objective, the model minimizes the distance between current activation $\mathbf{a}^{L^*}(x)$ and its corresponding target activation ($\mathbf{t}_k^{L^*}$ or $\mathbf{t}_u^{L^*}$). This process embeds the knowledge boundary into the weights themselves, eliminating the need for repeated steering at inference. Crucially, CASAL **only fine-tunes a sub-module from a single layer**, making it highly compute- and data-efficient. We conducted systematic ablation studies (Appendix K) to examine different fine-tuning strategies. Our results demonstrate that fine-tuning the different submodules of the MLP layer yields no statistically significant performance differences. Further details for the training process and hyperparameter research are included in Appendix D and L.

3 CASAL is Effective and Efficient

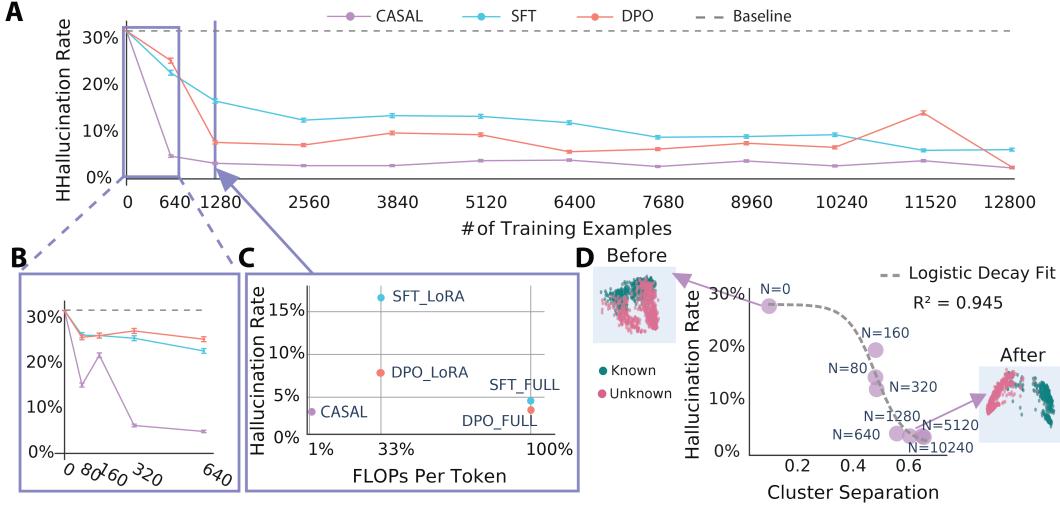


Figure 2: **CASAL is both sample efficient and compute efficient.** (A–B) CASAL achieves strong hallucination reduction with orders-of-magnitude fewer training examples comparing to LoRA-based fine-tuning with SFT and DPO. (C) CASAL is over $30\times$ more compute-efficient than PEFT baselines such as LoRA. (D) Hallucination reduction correlates with improved cluster separation between known and unknown queries, measured by silhouette score.

We evaluate CASAL against strong baselines including Supervised Fine-Tuning (SFT) and Direct Preference Optimization (DPO), which represent the predominant fine-tuning approaches deployed in production systems today (hyperparameters search and other training details are provided in Appendix M). By demonstrating CASAL’s superiority over these widely-adopted techniques, we establish its practical applicability for real-world deployment beyond toy settings.

3.1 Sample Efficiency

We quantify hallucination reduction performance primarily using the *hallucination rate*, which captures the fraction of unknown queries incorrectly attempted by the model. Figure 2 summarizes our key findings, with additional details on the hallucination rate metric provided in Appendix H.2. CASAL achieves substantially lower hallucination rates across a wide range of training set sizes. When trained on just 640 examples, CASAL already matches or surpasses the performance of SFT and DPO trained on 12,800 examples (Figure 2A–B). This translates into more than $20\times$ **higher data efficiency**, demonstrating that CASAL is especially practical in data-scarce settings.

3.2 Compute Efficiency

Beyond sample efficiency, CASAL is also highly compute efficient. By updating only a lightweight sub-module within a single transformer layer, CASAL is substantially more compute efficient than full fine-tuning or even LoRA-based parameter-efficient fine-tuning (PEFT). As shown in Figure 2C, CASAL achieves lower hallucination rates while requiring over $30\times$ **fewer FLOPs per token** than LoRA during training, underscoring its practicality for large-scale deployments. Details of FLOPs calculations are included in Appendix N.

3.3 Learning Better Knowledge Boundaries

By training with a local representation loss, CASAL encourages clearer separation between activations corresponding to known and unknown queries. We compute Silhouette score as a measure of cluster

Methods	Refusal Rate (\downarrow)			Accuracy (\uparrow)		
	PopQA	TriviaQA	EntityQA	PopQA	TriviaQA	EntityQA
Baseline	18.19% \pm 3.01	7.93% \pm 1.14	8.94% \pm 2.18	91.08% \pm 2.23	95.82% \pm 2.24	88.59% \pm 1.46
SFT	20.32% \pm 1.09	10.01% \pm 1.16	11.08% \pm 1.24	82.89% \pm 1.33	92.45% \pm 1.29	85.75% \pm 1.18
DPO	21.79% \pm 1.11	14.37% \pm 2.06	17.66% \pm 2.14	90.25%\pm1.06	95.30% \pm 0.96	89.84% \pm 1.16
CASAL	19.89%\pm1.15	7.29%\pm1.34	6.84%\pm1.23	85.11% \pm 1.88	95.34%\pm2.25	89.9%\pm0.99

Table 1: CASAL does not introduce over-refusal nor degrade performance for known queries. Refusal rate and accuracy across three different QA datasets are measured.

Methods	Accuracy (\uparrow)			Win rate (\uparrow)
	MMLU (General)	GSM8K (Math)	GPQA (Reasoning)	MT Bench (Coherence)
Baseline	68.01 \pm 0.34	77.48 \pm 1.15	33.31 \pm 0.34	7.38 \pm 0.06
SFT	67.90 \pm 0.23	75.66 \pm 1.18	32.82 \pm 0.34	7.44 \pm 0.05
DPO	68.03 \pm 0.26	78.16 \pm 1.14	31.43 \pm 0.37	7.39 \pm 0.05
CASAL	68.04 \pm 0.44	77.02 \pm 1.16	33.18 \pm 0.34	7.57 \pm 0.08

Table 2: CASAL preserves general capability. Performances (higher is better) on general capability, math, reasoning and context-aware conversational ability in multi-turn dialogues are measured.

separation. As shown in Figure 2D, Silhouette scores³ increase as training progresses, and this separation is correlated with the reduction in hallucination rate. The strong correspondence (logistic fit, $R^2 = 0.945$) between representational separation and behavioral outcomes indicates that CASAL’s effectiveness arises from more faithfully encoding and utilizing knowledge boundaries.

4 CASAL Preserves Model Capability

An important requirement for any practically useful hallucination-reduction method is that it should not degrade a model’s general capabilities nor induce excessive refusals on queries the model can correctly answer. We therefore evaluate CASAL across both refusal behavior and broad capability benchmarks. Table 1 reports refusal rates on three QA datasets. CASAL achieves the lowest refusal rates on TriviaQA (7.29%) and EntityQA (6.84%), while maintaining a competitive rate on PopQA (19.89%). These results demonstrate that CASAL reduces hallucination on unknown queries without over-penalizing the model into unnecessary refusals for known ones. We also evaluate against Contrastive Activation Addition (CAA), a popular inference-time steering method (Rimsky et al., 2024). As summarized in Section E, while CASAL achieves comparable hallucination rates to CAA on unknown queries, it maintains performance on known queries, whereas CAA degrades accuracy for questions the model could previously answer correctly. This finding aligns with previous work (Durmus et al., 2024; Chen et al., 2025b) showing that inference-time steering can introduce undesirable side effects.

We further assess models’ general capability, including MMLU for general knowledge, GSM8K for math reasoning, GPQA for scientific reasoning, and MT-Bench for coherence in multi-turn conversations. As shown in Table 2, CASAL performs on par with strong baselines across all metrics, matching the baseline on MMLU (Hendrycks et al., 2021), maintaining nearly identical scores on GSM8K (Cobbe et al., 2021) and GPQA (Rein et al., 2023), and achieving the best performance on MT-Bench (Zheng et al., 2023). Beyond these quantitative measures, we provide raw model outputs in Appendix F to allow readers to assess the natural flow and coherence of generated responses after CASAL training. These results demonstrate that CASAL reduces hallucinations on unknown queries while avoiding over-refusal on known queries, all without sacrificing general capability—a balance critical for practical deployment.

³To quantify the cluster separation, we use the Silhouette score (Rousseeuw, 1987), a standard metric that measures how similar an object is to its own cluster compared to other clusters. Further details can be found in Appendix H.4.

Dataset	Methods	Hallucination Rate (Unknown) (\downarrow)		Refusal Rate (Known) (\downarrow)		Accuracy (Known) (\uparrow)	
		Train	Test	Train	Test	Train	Test
TriviaQA		Wiki	Web	Wiki	Web	Wiki	Web
	Before CASAL	48.20% \pm 1.34	50.74% \pm 1.12	9.06% \pm 0.93	7.93% \pm 2.02	94.22% \pm 1.44	95.82% \pm 1.22
	After CASAL	20.47% \pm 1.31	32.42% \pm 1.29	8.28% \pm 1.16	11.69% \pm 2.22	92.03% \pm 0.82	90.08% \pm 1.33
PopQA		Group 1	Group 2	Group 1	Group 2	Group 1	Group 2
	Before CASAL	74.87% \pm 2.92	74.35% \pm 1.56	18.95% \pm 1.39	18.19% \pm 1.46	90.84% \pm 1.51	91.08% \pm 0.92
	After CASAL	22.48% \pm 1.45	23.42% \pm 1.94	13.97% \pm 1.78	19.10% \pm 1.30	85.23% \pm 0.86	84.27% \pm 1.99

Table 3: CASAL learns a generalizable notion of **known** vs. **unknown**, and can transfer between data sources within TriviaQA and generalize across groups within PopQA.

Methods	Hallucination Rate (\downarrow)		Refusal Rate (\downarrow)		Accuracy (\uparrow)	
	Train	Test	Train	Test	Train	Test
	TriviaQA	EntityQA	TriviaQA	EntityQA	TriviaQA	EntityQA
Before CASAL	48.2% \pm 1.33	50.74% \pm 0.92	9.06% \pm 1.22	12.89% \pm 1.49	94.22% \pm 0.93	95.82% \pm 2.32
After CASAL	28.83% \pm 1.53	11.72% \pm 1.66	9.29% \pm 1.48	13.82% \pm 1.55	93.36% \pm 1.47	95.77% \pm 1.64

Table 4: CASAL supports OOD generalization across different datasets. The model is trained on the TriviaQA dataset and tested on EntityQA as an out-of-distribution setting.

5 CASAL is OOD Generalizable

Beyond reducing hallucinations, it is essential that CASAL captures a generalizable notion of what the model knows versus does not know. We therefore test its ability to generalize across both in-distribution and out-of-distribution (OOD) settings. We first evaluate whether CASAL’s learned knowledge boundary transfers across different groups within the same dataset. As shown in Table 3, CASAL trained on Wikipedia-style data generalizes effectively to web data, reducing hallucination rate from 50.7% to 32.4% while maintaining high accuracy on known queries (92.0% vs. 95.8%). A similar trend is observed on PopQA (Table 3), where CASAL substantially reduces hallucinations in both Group 1 and Group 2, lowering test hallucination rates from 74.4% to 23.4%. These results indicate that CASAL does not simply memorize steering directions but learns a transferable notion of known versus unknown knowledge that holds across diverse data groups.

We next evaluate a stronger OOD setting: training CASAL on one dataset and testing it on a completely different one. Specifically, CASAL is trained on TriviaQA and evaluated on EntityQA (Table 4). Remarkably, hallucination rate on the unseen EntityQA dataset drops from 50.7% to 11.7%, while accuracy on known queries remains above 95%. This demonstrates that CASAL’s learned representations extend beyond the training domain, capturing knowledge boundaries that remain robust even under OOD transfer. Together, these results establish that CASAL generalizes well both across sub-groups within a dataset and across entirely distinct datasets. This robustness highlights that CASAL is not merely overfitting to a narrow training distribution but instead induces a broadly applicable mechanism for distinguishing known from unknown queries.

Methods	WorldCuisines Dataset		
	Unknown	Known	
	Hallucination Rate (\downarrow)	Refusal Rate (\downarrow)	Accuracy (\uparrow)
Before CASAL	72.35% \pm 1.77	13.91% \pm 1.37	76.72% \pm 1.67
After CASAL	33.34% \pm 3.13	25.44% \pm 2.91	90.36% \pm 1.96

Table 5: **CASAL is modality agnostic.** It reduces hallucination in vision-language model on WorldCuisines-VQA dataset.

6 CASAL is Modality and Architecture Agnostic

6.1 CASAL Reduces Hallucination in Vision-Language Models

We apply CASAL to a vision-language model: Qwen2.5-VL-7B-Instruct (Qwen et al., 2024) and perform training on the WorldCuisines-VQA (Winata et al., 2024) dataset. Finally, we evaluate whether CASAL generalizes beyond standard dense transformer architectures and text-only settings. CASAL reduces hallucination rate (Table 5) by 38.74%. Importantly, accuracy on known queries is preserved. This confirms that CASAL’s mechanism for sharpening knowledge boundaries is not tied to language-only models but extends naturally to multimodal models. Further details for training vision-language models are provided in Appendix O.

6.2 Effectiveness on Mixture-of-Experts Models

MoE models pose a unique challenge since knowledge and uncertainty may be distributed across different experts. We first ask "how are unknown versus known queries represented across experts?" Are certain experts specialized in representing known and others specialized in unknown? Or are they co-represented in the same experts? We started our investigation by visualizing the activations in different experts in the OLMoE model (Muennighoff et al., 2025). As illustrated in Figure 3A, activations for known and unknown queries are mostly co-represented in the same experts. Similar to dense model training, CASAL applies a local representation loss on the residual stream activations with converging signal across all experts (Figure 3B). After training, residual stream activations show a much clearer boundary between known and unknown queries (Figure 3C), which translates into significant improvements in hallucination rates. Hallucination rate for unknown queries drops by 42.9%, while accuracy on known queries remains unchanged (Figure 3D). Further details regarding the CASAL training for MoE models can be found in Appendix P. These results demonstrate that CASAL effectively extends to MoE architectures without sacrificing accuracy. Together, these results establish that CASAL is both *architecture-agnostic* and *modality-agnostic*. Whether applied to dense or MoE transformers, or to text-only versus vision-language models, CASAL consistently reduces hallucination rates while maintaining high accuracy and balanced refusal behavior. This broad applicability highlights CASAL’s potential as a scalable, general-purpose alignment technique.

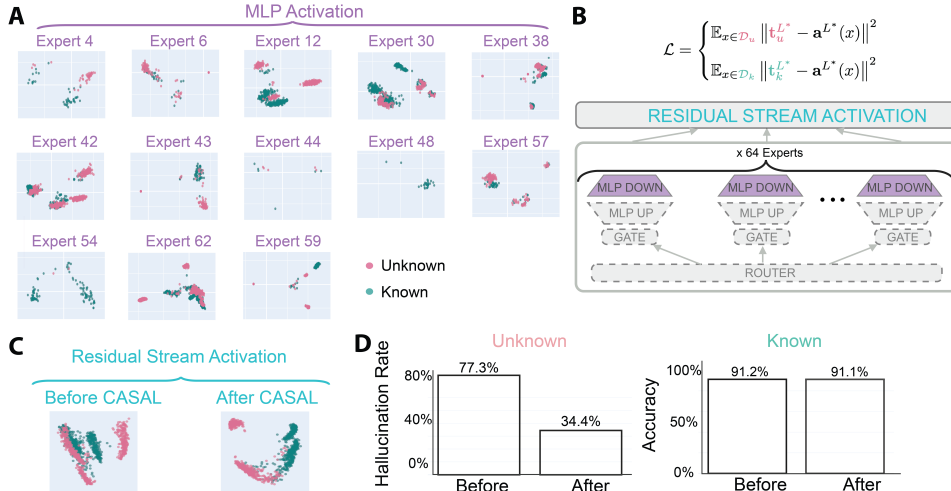


Figure 3: **CASAL is architecture-agnostic.** It effectively reduces hallucination for OLMoE. (A) Visualization of MLP activations from different experts in a MoE model before CASAL training. (B) CASAL applies a local representation loss on residual stream activations. During training, weights are updated on only a lightweight sub-module across experts. (C) Residual stream activations before and after CASAL training. (D) CASAL reduces hallucination rate on unknown queries while maintaining low refusal score and high accuracy for known queries.

7 Related Work

7.1 Hallucination Mitigation

Inference-time Intervention. Steering-based approaches (Rimsky et al., 2024; Turner et al., 2024) for hallucination reduction typically apply interventions during inference (Ferrando et al., 2025; Ji et al., 2025; Li et al., 2024; Park et al., 2025). While effective, this requires solving a local optimization problem for every input (e.g., shifting activations along a direction at every forward pass), introducing extra computational overhead during deployment to monitor and intervene. In contrast, CASAL eliminates the need for per-instance intervention by directly baking the knowledge boundaries into model parameters, enabling scalable deployment in production.

In-weight Learning. A complementary body of work modifies model parameters to encourage calibrated abstention and reduce hallucination. Early approaches train models to abstain from uncertain predictions via probabilistic calibration. Others focus on eliciting explicit confidence estimates in conversational models (Chen et al., 2024; Mielke et al., 2022). Concurrent work Chen et al. (2025b) proposes persona vector extraction, where finetuning steers models away from undesired persona directions. CASAL differs in two key ways: (i) rather than steering *away* from undesirable traits, we explicitly steer *towards* desirable representations (e.g., "abstaining" for unknowns, "compliance" for knowns); and (ii) CASAL presents an efficient training framework, yielding $\sim 30\times$ higher compute efficiency than state-of-the-art parameter-efficient finetuning methods such as LoRA.

7.2 Amortized Optimization, Activation Steering and Representation Learning

Amortized Optimization. Amortized optimization (Kingma and Welling, 2013; Rezende et al., 2014; Gershman and Goodman, 2014) is a widely used paradigm in which expensive, repeated optimization is replaced by training a parametric function that approximates the solution. Despite its influence in areas such as variational inference, sparse coding, gradient-based meta-learning and reinforcement learning (Amos, 2025; Chen et al., 2021), this perspective has been explored less in the context of interpretability or alignment (Paulus et al., 2025). CASAL can be viewed as *amortized activation steering*, where the resource intensive process of online steering is distilled into a lightweight subnetwork trained offline and reused at inference.

Activation Steering. A substantial line of work has focused on inference-time interventions, where steering vectors are applied dynamically to control model behavior without modifying weights (Ji et al., 2025; Li et al., 2024). Within this paradigm, a common approach to derive steering vectors is to construct sample pairs differing along a target concept and compute their difference-in-means (Arditi et al., 2024). Alternative methods further fine-tune the steering vectors to enable more effective behavior control with less side effect (Cao et al., 2024; Stickland et al., 2024; Parekh et al., 2025). Another line of work leverages sparse autoencoders (SAEs) to uncover interpretable features in an unsupervised manner, which can then serve as handles for steering interventions (Ferrando et al., 2025).

Representation Learning. A parallel line of work (Tian et al., 2025; Yu et al., 2024a; Chen et al., 2025b; Casademunt et al., 2025) focuses on shaping internal representations during finetuning to suppress undesired behaviors. Early methods include representation fine-tuning (ReFT), which encourages task-specific interventions on hidden states (Wu et al., 2024), and representation engineering (RepE), which monitors and manipulates high-level cognitive phenomena in LLMs (Zou et al., 2025). Other techniques explicitly control harmful states: Zou et al. (2024) introduce circuit breakers to block dangerous representations, while Yu et al. (2025) perform directional ablation of refusal features to maintain robustness under adversarial attacks. Similarly, Yousefpour et al. (2025) propose representation bending to disrupt harmful latent features. For unlearning, Shen et al. (2025b) train models to redirect unlearning data into refusal regions. Compared to these efforts, CASAL provides the *first* general steering-based training framework that is broadly applicable to **both dense and sparse (MoE) architectures**.

8 Conclusion and Limitations

In this work, we introduced CASAL, a lightweight, effective, and broadly applicable method for reducing hallucinations in large language models. By embedding knowledge boundaries directly into model weights, CASAL achieves substantial reductions in hallucination without degrading general capabilities, while being markedly more compute- and data-efficient than standard baselines. Beyond its empirical results, CASAL demonstrates a broader principle: insights from interpretability can be distilled into training objectives that scale.

While CASAL shows strong effectiveness and efficiency, several limitations remain. First, although CASAL generalizes across short-form QA datasets, modalities, and architectures, its effectiveness in reasoning models remains to be systematically tested. Second, our evaluation focuses specifically on hallucinations in short-form QA tasks. Exploring CASAL’s effectiveness in reducing hallucinations during long-form generations (Obeso et al., 2025) represents an important direction for future research. Finally, one particularly exciting future direction is the integration of CASAL into LLM-based agentic systems. As LLMs move toward becoming tool-using agents integrated into everyday workflows, their reliability becomes critical—misplaced confidence can lead to cascading errors with tangible consequences. While modern agents increasingly leverage external tools to address factual uncertainty, effective tool orchestration fundamentally depends on the agent’s ability to recognize the boundaries of its own knowledge. CASAL’s mechanism for sharpening these knowledge boundaries could therefore serve as a component for more reliable agentic systems, enabling agents to make better decisions about when to respond directly versus when to invoke tools such as web search or specialized APIs.

References

- Brandon Amos. Tutorial on amortized optimization, 2025. URL <https://arxiv.org/abs/2202.00665>.
- Andy Ardit, Oscar Obeso, Aaquib Syed, Daniel Paleka, Nina Panickssery, Wes Gurnee, and Neel Nanda. Refusal in language models is mediated by a single direction, 2024. URL <https://arxiv.org/abs/2406.11717>.
- Tom B. Brown, Benjamin Mann, Nick Ryder, Melanie Subbiah, Jared Kaplan, Prafulla Dhariwal, Arvind Neelakantan, Pranav Shyam, Girish Sastry, Amanda Askell, Sandhini Agarwal, Ariel Herbert-Voss, Gretchen Krueger, Tom Henighan, Rewon Child, Aditya Ramesh, Daniel M. Ziegler, Jeffrey Wu, Clemens Winter, Christopher Hesse, Mark Chen, Eric Sigler, Mateusz Litwin, Scott Gray, Benjamin Chess, Jack Clark, Christopher Berner, Sam McCandlish, Alec Radford, Ilya Sutskever, and Dario Amodei. Language models are few-shot learners, 2020. URL <https://arxiv.org/abs/2005.14165>.
- Yuanpu Cao, Tianrong Zhang, Bochuan Cao, Ziyi Yin, Lu Lin, Fenglong Ma, and Jinghui Chen. Personalized steering of large language models: Versatile steering vectors through bi-directional preference optimization. *Advances in Neural Information Processing Systems*, 37:49519–49551, 2024.
- Helena Casademunt, Caden Juang, Adam Karvonen, Samuel Marks, Senthoran Rajamanoharan, and Neel Nanda. Steering out-of-distribution generalization with concept ablation fine-tuning, 2025. URL <https://arxiv.org/abs/2507.16795>.
- Lida Chen, Zujie Liang, Xintao Wang, Jiaqing Liang, Yanghua Xiao, Feng Wei, Jinglei Chen, Zhenghong Hao, Bing Han, and Wei Wang. Teaching large language models to express knowledge boundary from their own signals, 2024. URL <https://arxiv.org/abs/2406.10881>.
- Lida Chen, Zujie Liang, Xintao Wang, Jiaqing Liang, Yanghua Xiao, Feng Wei, Jinglei Chen, Zhenghong Hao, Bing Han, and Wei Wang. Teaching large language models to express knowledge boundary from their own signals. In Yuji Zhang, Canyu Chen, Sha Li, Mor Geva, Chi Han, Xiaozhi Wang, Shangbin Feng, Silin Gao, Isabelle Augenstein, Mohit Bansal, Manling Li, and Heng Ji, editors, *Proceedings of the 3rd Workshop on Towards Knowledgeable Foundation Models (KnowFM)*, pages 26–39, Vienna, Austria, August 2025a. Association for Computational Linguistics. ISBN 979-8-89176-283-1. doi: 10.18653/v1/2025.knowllm-1.3. URL <https://aclanthology.org/2025.knowllm-1.3/>.
- Runjin Chen, Andy Ardit, Henry Sleight, Owain Evans, and Jack Lindsey. Persona vectors: Monitoring and controlling character traits in language models, 2025b. URL <https://arxiv.org/abs/2507.21509>.
- Tianlong Chen, Xiaohan Chen, Wuyang Chen, Howard Heaton, Jialin Liu, Zhangyang Wang, and Wotao Yin. Learning to optimize: A primer and a benchmark, 2021. URL <https://arxiv.org/abs/2103.12828>.
- Karl Cobbe, Vineet Kosaraju, Mohammad Bavarian, Mark Chen, Heewoo Jun, Lukasz Kaiser, Matthias Plappert, Jerry Tworek, Jacob Hilton, Reiichiro Nakano, Christopher Hesse, and John Schulman. Training verifiers to solve math word problems, 2021. URL <https://arxiv.org/abs/2110.14168>.
- Esin Durmus, Alex Tamkin, Jack Clark, Jerry Wei, Jonathan Marcus, Joshua Batson, Kunal Handa, Liane Lovitt, Meg Tong, Miles McCain, Oliver Rausch, Saffron Huang, Sam Bowman, Stuart Ritchie, Tom Henighan, and Deep Ganguli. Evaluating feature steering: A case study in mitigating social biases, 2024. URL <https://anthropic.com/research/evaluating-feature-steering>.
- Javier Ferrando, Oscar Obeso, Senthoran Rajamanoharan, and Neel Nanda. Do i know this entity? knowledge awareness and hallucinations in language models, 2025. URL <https://arxiv.org/abs/2411.14257>.

- Zorik Gekhman, Gal Yona, Roei Aharoni, Matan Eyal, Amir Feder, Roi Reichart, and Jonathan Herzig. Does fine-tuning llms on new knowledge encourage hallucinations? *arXiv preprint arXiv:2405.05904*, 2024a.
- Zorik Gekhman, Gal Yona, Roei Aharoni, Matan Eyal, Amir Feder, Roi Reichart, and Jonathan Herzig. Does fine-tuning llms on new knowledge encourage hallucinations?, 2024b. URL <https://arxiv.org/abs/2405.05904>.
- Samuel J. Gershman and Noah D. Goodman. Amortized inference in probabilistic reasoning. *Cognitive Science*, 38(1):69–100, 2014.
- Aaron Grattafiori, Abhimanyu Dubey, Abhinav Jauhri, Abhinav Pandey, Abhishek Kadian, Ahmad Al-Dahle, Aiesha Letman, Akhil Mathur, Alan Schelten, Alex Vaughan, Amy Yang, Angela Fan, Anirudh Goyal, Anthony Hartshorn, Aobo Yang, Archi Mitra, Archie Sravankumar, Artem Korenev, Arthur Hinsvark, Arun Rao, Aston Zhang, Aurelien Rodriguez, Austen Gregerson, Ava Spataru, Baptiste Roziere, Bethany Biron, Binh Tang, Bobbie Chern, Charlotte Caucheteux, Chaya Nayak, Chloe Bi, Chris Marra, Chris McConnell, Christian Keller, Christophe Touret, Chunyang Wu, Corinne Wong, Cristian Canton Ferrer, Cyrus Nikolaidis, Damien Allonsius, Daniel Song, Danielle Pintz, Danny Livshits, Danny Wyatt, David Esiobu, Dhruv Choudhary, Dhruv Mahajan, Diego Garcia-Olano, Diego Perino, Dieuwke Hupkes, Egor Lakomkin, Ehab AlBadawy, Elina Lobanova, Emily Dinan, Eric Michael Smith, Filip Radenovic, Francisco Guzmán, Frank Zhang, Gabriel Synnaeve, Gabrielle Lee, Georgia Lewis Anderson, Govind Thattai, Graeme Nail, Gregoire Mialon, Guan Pang, Guillem Cucurell, Hailey Nguyen, Hannah Korevaar, Hu Xu, Hugo Touvron, Iliyan Zarov, Imanol Arrieta Ibarra, Isabel Kloumann, Ishan Misra, Ivan Evtimov, Jack Zhang, Jade Copet, Jaewon Lee, Jan Geffert, Jana Vranes, Jason Park, Jay Mahadeokar, Jeet Shah, Jelmer van der Linde, Jennifer Billock, Jenny Hong, Jenya Lee, Jeremy Fu, Jianfeng Chi, Jianyu Huang, Jiawen Liu, Jie Wang, Jiecao Yu, Joanna Bitton, Joe Spisak, Jongsoo Park, Joseph Rocca, Joshua Johnstun, Joshua Saxe, Junteng Jia, Kalyan Vasuden Alwala, Karthik Prasad, Kartikeya Upasani, Kate Plawiak, Ke Li, Kenneth Heafield, Kevin Stone, Khalid El-Arini, Krithika Iyer, Kshitiz Malik, Kuenley Chiu, Kunal Bhalla, Kushal Lakhotia, Lauren Rantala-Yeary, Laurens van der Maaten, Lawrence Chen, Liang Tan, Liz Jenkins, Louis Martin, Lovish Madaan, Lubo Malo, Lukas Blecher, Lukas Landzaat, Luke de Oliveira, Madeline Muzzi, Mahesh Pasupuleti, Mannat Singh, Manohar Paluri, Marcin Kardas, Maria Tsimpoukelli, Mathew Oldham, Mathieu Rita, Maya Pavlova, Melanie Kambadur, Mike Lewis, Min Si, Mitesh Kumar Singh, Mona Hassan, Naman Goyal, Narjes Torabi, Nikolay Bashlykov, Nikolay Bogoychev, Niladri Chatterji, Ning Zhang, Olivier Duchenne, Onur Çelebi, Patrick Alrassy, Pengchuan Zhang, Pengwei Li, Petar Vasic, Peter Weng, Prajjwal Bhargava, Pratik Dubal, Praveen Krishnan, Punit Singh Koura, Puxin Xu, Qing He, Qingxiao Dong, Ragavan Srinivasan, Raj Ganapathy, Ramon Calderer, Ricardo Silveira Cabral, Robert Stojnic, Roberta Raileanu, Rohan Maheswari, Rohit Girdhar, Rohit Patel, Romain Sauvestre, Ronnie Polidoro, Roshan Sumbaly, Ross Taylor, Ruan Silva, Rui Hou, Rui Wang, Saghar Hosseini, Sahana Chennabasappa, Sanjay Singh, Sean Bell, Seohyun Sonia Kim, Sergey Edunov, Shao-liang Nie, Sharan Narang, Sharath Rapparthi, Sheng Shen, Shengye Wan, Shruti Bhosale, Shun Zhang, Simon Vandenhende, Soumya Batra, Spencer Whitman, Sten Sootla, Stephane Collet, Suchin Gururangan, Sydney Borodinsky, Tamar Herman, Tara Fowler, Tarek Sheasha, Thomas Georgiou, Thomas Scialom, Tobias Speckbacher, Todor Mihaylov, Tong Xiao, Ujjwal Karn, Vedanuj Goswami, Vibhor Gupta, Vignesh Ramanathan, Viktor Kerkez, Vincent Gonguet, Virginie Do, Vish Vogeti, Vitor Albiero, Vladan Petrovic, Weiwei Chu, Wenhan Xiong, Wenyin Fu, Whitney Meers, Xavier Martinet, Xiaodong Wang, Xiaofang Wang, Xiaoqing Ellen Tan, Xide Xia, Xinfeng Xie, Xuchao Jia, Xuwei Wang, Yaelle Goldschlag, Yashesh Gaur, Yasmine Babaei, Yi Wen, Yiwen Song, Yuchen Zhang, Yue Li, Yuning Mao, Zacharie Delpierre Coudert, Zheng Yan, Zhengxing Chen, Zoe Papakipos, Aaditya Singh, Aayushi Srivastava, Abha Jain, Adam Kelsey, Adam Shajnfeld, Adithya Gangidi, Adolfo Victoria, Ahuva Goldstand, Ajay Menon, Ajay Sharma, Alex Boesenberg, Alexei Baevski, Allie Feinstein, Amanda Kallet, Amit Sangani, Amos Teo, Anam Yunus, Andrei Lupu, Andres Alvarado, Andrew Caples, Andrew Gu, Andrew Ho, Andrew Poulton, Andrew Ryan, Ankit Ramchandani, Annie Dong, Annie Franco, Anuj Goyal, Aparajita Saraf, Arkabandhu Chowdhury, Ashley Gabriel, Ashwin Bharambe, Assaf Eisenman, Azadeh Yazdan, Beau James, Ben Maurer, Benjamin Leonhardi, Bernie Huang, Beth Loyd, Beto De Paola, Bhargavi Paranjape, Bing Liu, Bo Wu, Boyu Ni, Braden Hancock, Bram Wasti, Brandon Spence, Brani Stojkovic, Brian Gamido, Britt Montalvo, Carl Parker, Carly Burton, Catalina Mejia, Ce Liu, Changhan Wang, Changkyu Kim, Chao Zhou, Chester Hu, Ching-Hsiang Chu, Chris Cai, Chris Tindal, Christoph Feichtenhofer,

Cynthia Gao, Damon Civin, Dana Beaty, Daniel Kreymer, Daniel Li, David Adkins, David Xu, Davide Testuggine, Delia David, Devi Parikh, Diana Liskovich, Didem Foss, Dingkan Wang, Duc Le, Dustin Holland, Edward Dowling, Eissa Jamil, Elaine Montgomery, Eleonora Presani, Emily Hahn, Emily Wood, Eric-Tuan Le, Erik Brinkman, Esteban Arcaute, Evan Dunbar, Evan Smothers, Fei Sun, Felix Kreuk, Feng Tian, Filippas Kokkinos, Firat Ozgenel, Francesco Caggioni, Frank Kanayet, Frank Seide, Gabriela Medina Florez, Gabriella Schwarz, Gada Badeer, Georgia Swee, Gil Halpern, Grant Herman, Grigory Sizov, Guangyi, Zhang, Guna Lakshminarayanan, Hakan Inan, Hamid Shojanazeri, Han Zou, Hannah Wang, Hanwen Zha, Haroun Habeeb, Harrison Rudolph, Helen Suk, Henry Aspegren, Hunter Goldman, Hongyuan Zhan, Ibrahim Damlaj, Igor Molybog, Igor Tufanov, Ilias Leontiadis, Irina-Elena Veliche, Itai Gat, Jake Weissman, James Geboski, James Kohli, Janice Lam, Japhet Asher, Jean-Baptiste Gaya, Jeff Marcus, Jeff Tang, Jennifer Chan, Jenny Zhen, Jeremy Reizenstein, Jeremy Teboul, Jessica Zhong, Jian Jin, Jingyi Yang, Joe Cummings, Jon Carvill, Jon Shepard, Jonathan McPhie, Jonathan Torres, Josh Ginsburg, Junjie Wang, Kai Wu, Kam Hou U, Karan Saxena, Kartikay Khandelwal, Katayoun Zand, Kathy Matosich, Kaushik Veeraraghavan, Kelly Michelen, Keqian Li, Kiran Jagadeesh, Kun Huang, Kunal Chawla, Kyle Huang, Lailin Chen, Lakshya Garg, Lavender A, Leandro Silva, Lee Bell, Lei Zhang, Liangpeng Guo, Licheng Yu, Liron Moshkovich, Luca Wehrstedt, Madian Khabsa, Manav Avalani, Manish Bhatt, Martynas Mankus, Matan Hasson, Matthew Lennie, Matthias Reso, Maxim Groshev, Maxim Naumov, Maya Lathi, Meghan Keneally, Miao Liu, Michael L. Seltzer, Michal Valko, Michelle Restrepo, Mihir Patel, Mik Vyatskov, Mikayel Samvelyan, Mike Clark, Mike Macey, Mike Wang, Miquel Jubert Hermoso, Mo Metanat, Mohammad Rastegari, Munish Bansal, Nandhini Santhanam, Natascha Parks, Natasha White, Navyata Bawa, Nayan Singhal, Nick Egebo, Nicolas Usunier, Nikhil Mehta, Nikolay Pavlovich Laptev, Ning Dong, Norman Cheng, Oleg Chernoguz, Olivia Hart, Omkar Salpekar, Ozlem Kalinli, Parkin Kent, Parth Parekh, Paul Saab, Pavan Balaji, Pedro Rittner, Philip Bontrager, Pierre Roux, Piotr Dollar, Polina Zvyagina, Prashant Ratanchandani, Pritish Yuvraj, Qian Liang, Rachad Alao, Rachel Rodriguez, Rafi Ayub, Raghotham Murthy, Raghu Nayani, Rahul Mitra, Rangaprabhu Parthasarathy, Raymond Li, Rebekkah Hogan, Robin Battey, Rocky Wang, Russ Howes, Ruty Rinott, Sachin Mehta, Sachin Siby, Sai Jayesh Bondu, Samyak Datta, Sara Chugh, Sara Hunt, Sargun Dhillon, Sasha Sidorov, Satadru Pan, Saurabh Mahajan, Saurabh Verma, Seiji Yamamoto, Sharadh Ramaswamy, Shaun Lindsay, Sheng Feng, Shenghao Lin, Shengxin Cindy Zha, Shishir Patil, Shiva Shankar, Shuqiang Zhang, Shuqiang Zhang, Sinong Wang, Sneha Agarwal, Soji Sajuyigbe, Soumith Chintala, Stephanie Max, Stephen Chen, Steve Kehoe, Steve Satterfield, Sudarshan Govindaprasad, Sumit Gupta, Summer Deng, Sungmin Cho, Sunny Virk, Suraj Subramanian, Sy Choudhury, Sydney Goldman, Tal Remez, Tamar Glaser, Tamara Best, Thilo Koehler, Thomas Robinson, Tianhe Li, Tianjun Zhang, Tim Matthews, Timothy Chou, Tzook Shaked, Varun Vontimitta, Victoria Ajayi, Victoria Montanez, Vijai Mohan, Vinay Satish Kumar, Vishal Mangla, Vlad Ionescu, Vlad Poenaru, Vlad Tiberiu Mihailescu, Vladimir Ivanov, Wei Li, Wenchen Wang, Wenwen Jiang, Wes Bouaziz, Will Constable, Xiaocheng Tang, Xiaojian Wu, Xiaolan Wang, Xilun Wu, Xinbo Gao, Yaniv Kleinman, Yanjun Chen, Ye Hu, Ye Jia, Ye Qi, Yenda Li, Yilin Zhang, Ying Zhang, Yossi Adi, Youngjin Nam, Yu, Wang, Yu Zhao, Yuchen Hao, Yundi Qian, Yunlu Li, Yuzi He, Zach Rait, Zachary DeVito, Zef Rosnbrick, Zhaoduo Wen, Zhenyu Yang, Zhiwei Zhao, and Zhiyu Ma. The llama 3 herd of models, 2024. URL <https://arxiv.org/abs/2407.21783>.

Dan Hendrycks, Collin Burns, Steven Basart, Andy Zou, Mantas Mazeika, Dawn Song, and Jacob Steinhardt. Measuring massive multitask language understanding, 2021. URL <https://arxiv.org/abs/2009.03300>.

Ziwei Ji, Lei Yu, Yeskendir Koishekenov, Yejin Bang, Anthony Hartshorn, Alan Schelten, Cheng Zhang, Pascale Fung, and Nicola Cancedda. Calibrating verbal uncertainty as a linear feature to reduce hallucinations, 2025. URL <https://arxiv.org/abs/2503.14477>.

Mandar Joshi, Eunsol Choi, Daniel S. Weld, and Luke Zettlemoyer. Triviaqa: A large scale distantly supervised challenge dataset for reading comprehension, 2017a. URL <https://arxiv.org/abs/1705.03551>.

Mandar Joshi, Eunsol Choi, Daniel S. Weld, and Luke Zettlemoyer. Triviaqa: A large scale distantly supervised challenge dataset for reading comprehension, 2017b. URL <https://arxiv.org/abs/1705.03551>.

- Saurav Kadavath, Tom Conerly, Amanda Askell, Tom Henighan, Dawn Drain, Ethan Perez, Nicholas Schiefer, Zac Hatfield-Dodds, Nova DasSarma, Eli Tran-Johnson, Scott Johnston, Sheer El-Showk, Andy Jones, Nelson Elhage, Tristan Hume, Anna Chen, Yuntao Bai, Sam Bowman, Stanislav Fort, Deep Ganguli, Danny Hernandez, Josh Jacobson, Jackson Kernion, Shauna Kravec, Liane Lovitt, Kamal Ndousse, Catherine Olsson, Sam Ringer, Dario Amodei, Tom Brown, Jack Clark, Nicholas Joseph, Ben Mann, Sam McCandlish, Chris Olah, and Jared Kaplan. Language models (mostly) know what they know, 2022. URL <https://arxiv.org/abs/2207.05221>.
- Adam Tauman Kalai, Ofir Nachum, Santosh S. Vempala, and Edwin Zhang. Why language models hallucinate, 2025. URL <https://arxiv.org/abs/2509.04664>.
- Jared Kaplan, Sam McCandlish, Tom Henighan, Tom B. Brown, Benjamin Chess, Rewon Child, Scott Gray, Alec Radford, Jeffrey Wu, and Dario Amodei. Scaling laws for neural language models, 2020. URL <https://arxiv.org/abs/2001.08361>.
- Diederik P. Kingma and Max Welling. Auto-encoding variational bayes. *arXiv preprint arXiv:1312.6114*, 2013.
- Kenneth Li, Oam Patel, Fernanda Viégas, Hanspeter Pfister, and Martin Wattenberg. Inference-time intervention: Eliciting truthful answers from a language model, 2024. URL <https://arxiv.org/abs/2306.03341>.
- Moxin Li, Yong Zhao, Wenxuan Zhang, Shuaiyi Li, Wenya Xie, See-Kiong Ng, Tat-Seng Chua, and Yang Deng. Knowledge boundary of large language models: A survey. In *Proceedings of the 63rd Annual Meeting of the Association for Computational Linguistics (ACL 2025)*. Association for Computational Linguistics, 2025a. URL <https://aclanthology.org/2025.acl-long.256>. Also available as arXiv:2412.12472.
- Moxin Li, Yong Zhao, Wenxuan Zhang, Shuaiyi Li, Wenya Xie, See-Kiong Ng, Tat-Seng Chua, and Yang Deng. Knowledge boundary of large language models: A survey. In *Proceedings of the 63rd Annual Meeting of the Association for Computational Linguistics (ACL 2025)*. Association for Computational Linguistics, 2025b. URL <https://aclanthology.org/2025.acl-long.256>. Also available as arXiv:2412.12472.
- Alex Mallen, Akari Asai, Victor Zhong, Rajarshi Das, Daniel Khashabi, and Hannaneh Hajishirzi. When not to trust language models: Investigating effectiveness of parametric and non-parametric memories, 2023a. URL <https://arxiv.org/abs/2212.10511>.
- Alex Mallen, Akari Asai, Victor Zhong, Rajarshi Das, Daniel Khashabi, and Hannaneh Hajishirzi. When not to trust language models: Investigating effectiveness of parametric and non-parametric memories, 2023b. URL <https://arxiv.org/abs/2212.10511>.
- Kenneth Marino, Mohammad Rastegari, Ali Farhadi, and Roozbeh Mottaghi. OK-VQA: A visual question answering benchmark requiring external knowledge. *CoRR*, abs/1906.00067, 2019. URL <http://arxiv.org/abs/1906.00067>.
- Sabrina J. Mielke, Arthur Szlam, Emily Dinan, and Y-Lan Boureau. Reducing conversational agents’ overconfidence through linguistic calibration, 2022. URL <https://arxiv.org/abs/2012.14983>.
- Tomas Mikolov, Wen-tau Yih, and Geoffrey Zweig. Linguistic regularities in continuous space word representations. In Lucy Vanderwende, Hal Daumé III, and Katrin Kirchhoff, editors, *Proceedings of the 2013 Conference of the North American Chapter of the Association for Computational Linguistics: Human Language Technologies*, pages 746–751, Atlanta, Georgia, June 2013. Association for Computational Linguistics. URL <https://aclanthology.org/N13-1090>.
- Niklas Muennighoff, Luca Soldaini, Dirk Groeneveld, Kyle Lo, Jacob Morrison, Sewon Min, Weijia Shi, Pete Walsh, Oyvind Tafjord, Nathan Lambert, Yuling Gu, Shane Arora, Akshita Bhagia, Dustin Schwenk, David Wadden, Alexander Wettig, Binyuan Hui, Tim Dettmers, Douwe Kiela, Ali Farhadi, Noah A. Smith, Pang Wei Koh, Amanpreet Singh, and Hannaneh Hajishirzi. Olmoe: Open mixture-of-experts language models, 2025. URL <https://arxiv.org/abs/2409.02060>.

Neel Nanda, Andrew Lee, and Martin Wattenberg. Emergent linear representations in world models of self-supervised sequence models. In Yonatan Belinkov, Sophie Hao, Jaap Jumelet, Najoung Kim, Arya McCarthy, and Hosein Mohebbi, editors, *Proceedings of the 6th BlackboxNLP Workshop: Analyzing and Interpreting Neural Networks for NLP*, pages 16–30, Singapore, December 2023. Association for Computational Linguistics. doi: 10.18653/v1/2023.blackboxnlp-1.2. URL <https://aclanthology.org/2023.blackboxnlp-1.2>.

Oscar Obeso, Andy Arditi, Javier Ferrando, Joshua Freeman, Cameron Holmes, and Neel Nanda. Real-time detection of hallucinated entities in long-form generation, 2025. URL <https://arxiv.org/abs/2509.03531>.

OpenAI, Josh Achiam, Steven Adler, Sandhini Agarwal, Lama Ahmad, Ilge Akkaya, Florencia Leoni Aleman, Diogo Almeida, Janko Altenschmidt, Sam Altman, Shyamal Anadkat, Red Avila, Igor Babuschkin, Suchir Balaji, Valerie Balcom, Paul Baltescu, Haiming Bao, Mohammad Bavarian, Jeff Belgum, Irwan Bello, Jake Berdine, Gabriel Bernadett-Shapiro, Christopher Berner, Lenny Bogdonoff, Oleg Boiko, Madelaine Boyd, Anna-Luisa Brakman, Greg Brockman, Tim Brooks, Miles Brundage, Kevin Button, Trevor Cai, Rosie Campbell, Andrew Cann, Brittany Carey, Chelsea Carlson, Rory Carmichael, Brooke Chan, Che Chang, Fotis Chantzis, Derek Chen, Sully Chen, Ruby Chen, Jason Chen, Mark Chen, Ben Chess, Chester Cho, Casey Chu, Hyung Won Chung, Dave Cummings, Jeremiah Currier, Yunxing Dai, Cory Decareaux, Thomas Degry, Noah Deutsch, Damien Deville, Arka Dhar, David Dohan, Steve Dowling, Sheila Dunning, Adrien Ecoffet, Atty Eleti, Tyna Eloundou, David Farhi, Liam Fedus, Niko Felix, Simón Posada Fishman, Juston Forte, Isabella Fulford, Leo Gao, Elie Georges, Christian Gibson, Vik Goel, Tarun Gogineni, Gabriel Goh, Rapha Gontijo-Lopes, Jonathan Gordon, Morgan Grafstein, Scott Gray, Ryan Greene, Joshua Gross, Shixiang Shane Gu, Yufei Guo, Chris Hallacy, Jesse Han, Jeff Harris, Yuchen He, Mike Heaton, Johannes Heidecke, Chris Hesse, Alan Hickey, Wade Hickey, Peter Hoeschele, Brandon Houghton, Kenny Hsu, Shengli Hu, Xin Hu, Joost Huizinga, Shantanu Jain, Shawn Jain, Joanne Jang, Angela Jiang, Roger Jiang, Haozhun Jin, Denny Jin, Shino Jomoto, Billie Jonn, Heewoo Jun, Tomer Kaftan, Łukasz Kaiser, Ali Kamali, Ingmar Kanitscheider, Nitish Shirish Keskar, Tabarak Khan, Logan Kilpatrick, Jong Wook Kim, Christina Kim, Yongjik Kim, Jan Hendrik Kirchner, Jamie Kiros, Matt Knight, Daniel Kokotajlo, Łukasz Kondraciuk, Andrew Kondrich, Aris Konstantinidis, Kyle Kosic, Gretchen Krueger, Vishal Kuo, Michael Lampe, Ikai Lan, Teddy Lee, Jan Leike, Jade Leung, Daniel Levy, Chak Ming Li, Rachel Lim, Molly Lin, Stephanie Lin, Mateusz Litwin, Theresa Lopez, Ryan Lowe, Patricia Lue, Anna Makanju, Kim Malfacini, Sam Manning, Todor Markov, Yaniv Markovski, Bianca Martin, Katie Mayer, Andrew Mayne, Bob McGrew, Scott Mayer McKinney, Christine McLeavey, Paul McMillan, Jake McNeil, David Medina, Aalok Mehta, Jacob Menick, Luke Metz, Andrey Mishchenko, Pamela Mishkin, Vinnie Monaco, Evan Morikawa, Daniel Mossing, Tong Mu, Mira Murati, Oleg Murk, David Mély, Ashvin Nair, Reiichiro Nakano, Rajeev Nayak, Arvind Neelakantan, Richard Ngo, Hyeonwoo Noh, Long Ouyang, Cullen O’Keefe, Jakub Pachocki, Alex Paino, Joe Palermo, Ashley Pantuliano, Giambattista Parascandolo, Joel Parish, Emy Parparita, Alex Passos, Mikhail Pavlov, Andrew Peng, Adam Perelman, Filipe de Avila Belbute Peres, Michael Petrov, Henrique Ponde de Oliveira Pinto, Michael, Pokorný, Michelle Pokrass, Vitchyr H. Pong, Tolly Powell, Alethea Power, Boris Power, Elizabeth Proehl, Raul Puri, Alec Radford, Jack Rae, Aditya Ramesh, Cameron Raymond, Francis Real, Kendra Rimbach, Carl Ross, Bob Rotsted, Henri Roussez, Nick Ryder, Mario Saltarelli, Ted Sanders, Shibani Santurkar, Girish Sastry, Heather Schmidt, David Schnurr, John Schulman, Daniel Selsam, Kyla Sheppard, Toki Sherbakov, Jessica Shieh, Sarah Shoker, Pranav Shyam, Szymon Sidor, Eric Sigler, Maddie Simens, Jordan Sitkin, Katarina Slama, Ian Sohl, Benjamin Sokolowsky, Yang Song, Natalie Staudacher, Felipe Petroski Such, Natalie Summers, Ilya Sutskever, Jie Tang, Nikolas Tezak, Madeleine B. Thompson, Phil Tillet, Amin Tootoonchian, Elizabeth Tseng, Preston Tuggle, Nick Turley, Jerry Tworek, Juan Felipe Cerón Uribe, Andrea Vallone, Arun Vijayvergiya, Chelsea Voss, Carroll Wainwright, Justin Jay Wang, Alvin Wang, Ben Wang, Jonathan Ward, Jason Wei, CJ Weinmann, Akila Welihinda, Peter Welinder, Jiayi Weng, Lilian Weng, Matt Wiethoff, Dave Willner, Clemens Winter, Samuel Wolrich, Hannah Wong, Lauren Workman, Sherwin Wu, Jeff Wu, Michael Wu, Kai Xiao, Tao Xu, Sarah Yoo, Kevin Yu, Qiming Yuan, Wojciech Zaremba, Rowan Zellers, Chong Zhang, Marvin Zhang, Shengjia Zhao, Tianhao Zheng, Juntang Zhuang, William Zhuk, and Barret Zoph. Gpt-4 technical report, 2024. URL <https://arxiv.org/abs/2303.08774>.

- Long Ouyang, Jeff Wu, Xu Jiang, Diogo Almeida, Carroll L. Wainwright, Pamela Mishkin, Chong Zhang, Sandhini Agarwal, Katarina Slama, Alex Ray, John Schulman, Jacob Hilton, Fraser Kelton, Luke Miller, Maddie Simens, Amanda Askell, Peter Welinder, Paul Christiano, Jan Leike, and Ryan Lowe. Training language models to follow instructions with human feedback, 2022. URL <https://arxiv.org/abs/2203.02155>.
- Gerry Pallier, Rebecca Wilkinson, Vanessa Danthiir, Sabina Kleitman, Goran Knezevic, Lazar Stankov, and Richard D. Roberts. The role of individual differences in the accuracy of confidence judgments. *The Journal of General Psychology*, 129(3):257–299, July 2002. doi: 10.1080/00221300209602099.
- Jayneel Parekh, Pegah Khayatan, Mustafa Shukor, Arnaud Dapogny, Alasdair Newson, and Matthieu Cord. Learning to steer: Input-dependent steering for multimodal llms. *arXiv preprint arXiv:2508.12815*, 2025.
- Kiho Park, Yo Joong Choe, and Victor Veitch. The linear representation hypothesis and the geometry of large language models, 2023. URL <https://arxiv.org/abs/2311.03658>.
- Seongheon Park, Xuefeng Du, Min-Hsuan Yeh, Haobo Wang, and Yixuan Li. Steer llm latents for hallucination detection, 2025. URL <https://arxiv.org/abs/2503.01917>.
- Anselm Paulus, Arman Zharmagambetov, Chuan Guo, Brandon Amos, and Yuandong Tian. Advprompter: Fast adaptive adversarial prompting for llms, 2025. URL <https://arxiv.org/abs/2404.16873>.
- Qwen, :, An Yang, Baosong Yang, Beichen Zhang, Binyuan Hui, Bo Zheng, Bowen Yu, Chengyuan Li, Dayiheng Liu, Fei Huang, Haoran Wei, Huan Lin, Jian Yang, Jianhong Tu, Jianwei Zhang, Jianxin Yang, Jiaxi Yang, Jingren Zhou, Junyang Lin, Kai Dang, Keming Lu, Keqin Bao, Kexin Yang, Le Yu, Mei Li, Mingfeng Xue, Pei Zhang, Qin Zhu, Rui Men, Runji Lin, Tianhao Li, Tianyi Tang, Tingyu Xia, Xingzhang Ren, Xuancheng Ren, Yang Fan, Yang Su, Yichang Zhang, Yu Wan, Yuqiong Liu, Zeyu Cui, Zhenru Zhang, and Zihan Qiu. Qwen2.5 technical report, 2025. URL <https://arxiv.org/abs/2412.15115>.
- A Yang Qwen, Baosong Yang, B Zhang, B Hui, B Zheng, B Yu, Chengpeng Li, D Liu, F Huang, H Wei, et al. Qwen2. 5 technical report. *arXiv preprint*, 2024.
- Vipula Rawte, Amit Sheth, and Amitava Das. A survey of hallucination in large foundation models. *arXiv preprint arXiv:2309.05922*, 2023.
- David Rein, Betty Li Hou, Asa Cooper Stickland, Jackson Petty, Richard Yuanzhe Pang, Julien Dirani, Julian Michael, and Samuel R. Bowman. Gpqa: A graduate-level google-proof q&a benchmark, 2023. URL <https://arxiv.org/abs/2311.12022>.
- Danilo Jimenez Rezende, Shakir Mohamed, and Daan Wierstra. Stochastic backpropagation and approximate inference in deep generative models. In *Proceedings of the 31st International Conference on Machine Learning*, pages 1278–1286, 2014.
- Nina Rimskey, Nick Gabrieli, Julian Schulz, Meg Tong, Evan Hubinger, and Alexander Turner. Steering llama 2 via contrastive activation addition. In Lun-Wei Ku, Andre Martins, and Vivek Srikumar, editors, *Proceedings of the 62nd Annual Meeting of the Association for Computational Linguistics (Volume 1: Long Papers)*, pages 15504–15522, Bangkok, Thailand, August 2024. Association for Computational Linguistics. doi: 10.18653/v1/2024.acl-long.828. URL <https://aclanthology.org/2024.acl-long.828/>.
- Peter J Rousseeuw. Silhouettes: a graphical aid to the interpretation and validation of cluster analysis. *Journal of Computational and Applied Mathematics*, 20:53–65, 1987.
- William F Shen, Xinchu Qiu, Nicola Cancedda, and Nicholas D Lane. Don’t make it up: Preserving ignorance awareness in llm fine-tuning. *arXiv preprint arXiv:2506.14387*, 2025a.
- William F. Shen, Xinchu Qiu, Meghdad Kurmanji, Alex Jacob, Lorenzo Sani, Yihong Chen, Nicola Cancedda, and Nicholas D. Lane. Lunar: Llm unlearning via neural activation redirection, 2025b. URL <https://arxiv.org/abs/2502.07218>.

- Lazar Stankov and John D. Crawford. Confidence judgments in studies of individual differences. *Personality and Individual Differences*, 21(6):971–986, 1996. ISSN 0191-8869. doi: 10.1016/S0191-8869(96)00130-4.
- Asa Cooper Stickland, Alexander Lyzhov, Jacob Pfau, Salsabila Mahdi, and Samuel R Bowman. Steering without side effects: Improving post-deployment control of language models. *arXiv preprint arXiv:2406.15518*, 2024.
- Adly Templeton, Tom Conerly, Jonathan Marcus, Jack Lindsey, Trenton Bricken, Brian Chen, Adam Pearce, Craig Citro, Emmanuel Ameisen, Andy Jones, Hoagy Cunningham, Nicholas L Turner, Callum McDougall, Monte MacDiarmid, Alex Tamkin, Esin Durmus, Tristan Hume, Francesco Mosconi, C. Daniel Freeman, Theodore R. Sumers, Edward Rees, Joshua Batson, Adam Jermy, Shan Carter, Chris Olah, and Tom Henighan. Scaling monosemanticity: Extracting interpretable features from claude 3 sonnet, 2024. URL <https://transformer-circuits.pub/2024/scaling-monosemanticity/index.html>. Accessed: 2025-09-22.
- Bowei Tian, Xuntao Lyu, Meng Liu, Hongyi Wang, and Ang Li. Why representation engineering works: A theoretical and empirical study in vision-language models, 2025. URL <https://arxiv.org/abs/2503.22720>.
- Alexander Matt Turner, Lisa Thiergart, Gavin Leech, David Udell, Juan J. Vazquez, Ulisse Mini, and Monte MacDiarmid. Steering language models with activation engineering, 2024. URL <https://arxiv.org/abs/2308.10248>.
- Jason Wei, Nguyen Karina, Hyung Won Chung, Yunxin Joy Jiao, Spencer Papay, Amelia Glaese, John Schulman, and William Fedus. Measuring short-form factuality in large language models, 2024. URL <https://arxiv.org/abs/2411.04368>.
- Genta Indra Winata, Frederikus Hudi, Patrick Amadeus Irawan, David Anugraha, Rifki Afina Putri, Yutong Wang, Adam Nohejl, Ubaidillah Ariq Prathama, Nedjma Ousidhoum, Afifa Amriani, et al. Worldcuisines: A massive-scale benchmark for multilingual and multicultural visual question answering on global cuisines. *arXiv preprint arXiv:2410.12705*, 2024.
- Zhengxuan Wu, Aryaman Arora, Zheng Wang, Atticus Geiger, Dan Jurafsky, Christopher D. Manning, and Christopher Potts. Reft: Representation finetuning for language models, 2024. URL <https://arxiv.org/abs/2404.03592>.
- Wannan Yang and György Buzsáki. Interpretability of LLM deception: Universal motif. In *ICLR 2025 Conference*, 2025. URL <https://openreview.net/forum?id=znL549Ymoi>. Submitted Sept 28, 2024; Last modified Feb 5, 2025; ICLR 2025 submission, under review.
- Zhangyue Yin, Qiushi Sun, Qipeng Guo, Jiawen Wu, Xipeng Qiu, and Xuanjing Huang. Do large language models know what they don’t know? In *Findings of the Association for Computational Linguistics (ACL 2023)*, 2023a. URL <https://aclanthology.org/2023.findings-acl.551/>.
- Zhangyue Yin, Qiushi Sun, Qipeng Guo, Jiawen Wu, Xipeng Qiu, and Xuanjing Huang. Do large language models know what they don’t know?, 2023b. URL <https://arxiv.org/abs/2305.18153>.
- Gal Yona, Roei Aharoni, and Mor Geva. Can large language models faithfully express their intrinsic uncertainty in words?, 2024. URL <https://arxiv.org/abs/2405.16908>.
- Ashkan Yousefpour, Taeheon Kim, Ryan S. Kwon, Seungbeen Lee, Wonje Jeung, Seungju Han, Alvin Wan, Harrison Ngan, Youngjae Yu, and Jonghyun Choi. Representation bending for large language model safety, 2025. URL <https://arxiv.org/abs/2504.01550>.
- Lei Yu, Meng Cao, Jackie Chi Kit Cheung, and Yue Dong. Mechanistic understanding and mitigation of language model non-factual hallucinations. In *Findings of the Association for Computational Linguistics: EMNLP 2024*, pages 7943–7956, 2024a.
- Lei Yu, Meng Cao, Jackie Chi Kit Cheung, and Yue Dong. Mechanistic understanding and mitigation of language model non-factual hallucinations. *arXiv preprint arXiv:2403.18167*, 2024b. doi: 10.48550/arXiv.2403.18167.

- Lei Yu, Virginie Do, Karen Hambardzumyan, and Nicola Cancedda. Robust llm safeguarding via refusal feature adversarial training, 2025. URL <https://arxiv.org/abs/2409.20089>.
- Anqi Zhang, Yulin Chen, Jane Pan, Chen Zhao, Aurojit Panda, Jinyang Li, and He He. Reasoning models know when they’re right: Probing hidden states for self-verification, 2025. URL <https://arxiv.org/abs/2504.05419>.
- Lianmin Zheng, Wei-Lin Chiang, Ying Sheng, Siyuan Zhuang, Zhanghao Wu, Yonghao Zhuang, Zi Lin, Zhuohan Li, Dacheng Li, Eric P. Xing, Hao Zhang, Joseph E. Gonzalez, and Ion Stoica. Judging llm-as-a-judge with mt-bench and chatbot arena, 2023. URL <https://arxiv.org/abs/2306.05685>.
- Andy Zou, Long Phan, Justin Wang, Derek Duenas, Maxwell Lin, Maksym Andriushchenko, Rowan Wang, Zico Kolter, Matt Fredrikson, and Dan Hendrycks. Improving alignment and robustness with circuit breakers, 2024. URL <https://arxiv.org/abs/2406.04313>.
- Andy Zou, Long Phan, Sarah Chen, James Campbell, Phillip Guo, Richard Ren, Alexander Pan, Xuwang Yin, Mantas Mazeika, Ann-Kathrin Dombrowski, Shashwat Goel, Nathaniel Li, Michael J. Byun, Zifan Wang, Alex Mallen, Steven Basart, Sanmi Koyejo, Dawn Song, Matt Fredrikson, J. Zico Kolter, and Dan Hendrycks. Representation engineering: A top-down approach to ai transparency, 2025. URL <https://arxiv.org/abs/2310.01405>.

Appendix

Table of Contents

A	Further Discussion on Related Work	20
A.1	Knowledge Representation and the Linear Representation Hypothesis	20
B	Further Discussion on Amortized Optimization	20
C	Steering	22
C.1	Steering Vector Construction	22
C.2	Layer Selection	22
D	CASAL Training	23
D.1	Relationship between Activation Steering and CASAL Training	23
D.2	Weight Update before and after CASAL	24
E	Contrastive Activation Addition (CAA) VS CASAL	25
F	Example Model Outputs	26
G	Dataset	33
G.1	Entity Dataset	33
G.2	TriviaQA Dataset	34
G.3	PopQA Dataset	34
G.4	WorldCuisines Dataset	34
H	Metrics for Performance and Cluster Separation	35
H.1	Refusal Rate	35
H.2	Hallucination Rate	35
H.3	Accuracy	35
H.4	Silhouette Score	35
I	Knowledge Probing	37
I.1	Knowledge Probing Threshold	39
J	Models	39
K	Ablation	40
K.1	Sub-module for training	40
L	Hyper-parameter Search for CASAL Training	40
L.1	Learning Rate	41
L.2	Steering Strength	41
M	SFT and DPO Training	42

N	Compute Cost of Calculation (FLOPs per Token)	43
N.1	Full-parameter finetuning	43
N.2	Comparing full-parameter finetune and CASAL finetune	43
N.3	LoRA finetuning	44
N.4	Comparing full-parameter finetune and LoRA finetune	45
O	Multimodal Model	48
P	Mixture-of-Experts (MoE) Training	49
P.1	PCA Activation Across Experts	51
Q	Computational Requirements	52

A Further Discussion on Related Work

A.1 Knowledge Representation and the Linear Representation Hypothesis

Humans often display systematic overconfidence: their subjective confidence often exceeds objective accuracy (Pallier et al., 2002; Stankov and Crawford, 1996). Large language models (LLMs) exhibit a similar pattern: they are poorly calibrated on general knowledge tasks, frequently producing answers with misplaced confidence (Kadavath et al., 2022; Yin et al., 2023b; Yona et al., 2024; Zhang et al., 2025).

Recent interpretability studies (using sparse autoencoder (SAE) features (Ferrando et al., 2025) or residual stream activations (Ji et al., 2025)) suggest that transformer models encode many abstract concepts as linear directions in activation space (Nanda et al., 2023; Mikolov et al., 2013; Park et al., 2023; Arditì et al., 2024; Yang and Buzsáki, 2025). Behavioral traits such as truthfulness, sycophancy, refusal (Arditì et al., 2024), and reasoning strategies have shown to be linearly represented. Emerging evidence indicates that models may also possess intrinsic linear representations of knowledge boundary (Ferrando et al., 2025) and uncertainty (Ji et al., 2025) for their own knowledge limitation, which can be harnessed for calibrating overconfidence in LLMs.

B Further Discussion on Amortized Optimization

Amortized Optimization Perspective. Our approach combines insights from interpretability and amortized optimization (Kingma and Welling, 2013; Rezende et al., 2014; Gershman and Goodman, 2014). Formally, amortized optimization replaces repeated problem-specific optimizations

$$\theta^*(x) = \arg \min_{\theta} \mathcal{L}(f_{\theta}, x)$$

with the training of a parametric function $g_{\phi}(x)$ that directly predicts an approximate solution, i.e., $\theta^*(x) \approx g_{\phi}(x)$. This paradigm reduces per-instance optimization compute cost by learning a global set of parameters ϕ that amortize inference across the data distribution.

VAEs provide a canonical example: instead of optimizing a separate variational posterior $q(z|x)$ for every datapoint, the encoder $q_{\phi}(z|x)$ is trained to amortize inference. The optimization signal is the evidence lower bound (ELBO),

$$\mathcal{L}_{\text{ELBO}}(\theta, \phi) = \mathbb{E}_{q_{\phi}(z|x)}[\log p_{\theta}(x|z)] - \text{KL}(q_{\phi}(z|x) \parallel p(z)),$$

Amortization arises from the parameterization of inference with a shared encoder network $q_{\phi}(z|x)$, which maps each input x to distributional parameters in a single forward pass, replacing the need to optimize separate variational parameters for each datapoint.

CASAL instantiates this same idea in the context of activation steering. Instead of repeatedly solving for a steering direction $v^*(x)$ that separates known from unknown knowledge in residual activations

$h(x)$, we train a lightweight subnetwork s_ϕ to approximate this solution:

$$v^*(x) \approx s_\phi(h(x)).$$

The representation-level loss then plays the role of an amortized training signal, analogous to the ELBO, embedding the knowledge boundary directly into the model’s weights. This allows the model to align its outputs with its internal representations in a single forward pass, making steering efficient and scalable.

C Steering

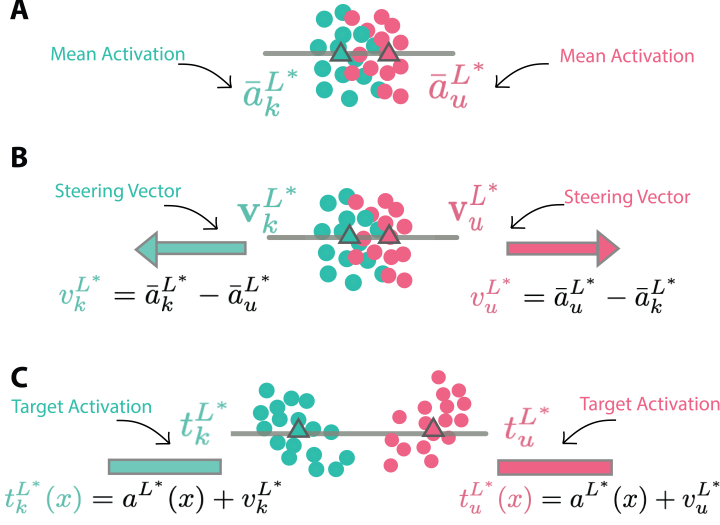


Figure 4: **Illustration of steering vector and target activation construction.** (A) Mean activations at the target layer L^* are computed for **known queries** (\bar{a}_k^{L*}) and **unknown queries** (\bar{a}_u^{L*}). (B) Steering vectors are defined by the difference of these means: $v_k^{L*} = \bar{a}_k^{L*} - \bar{a}_u^{L*}$ (pointing toward the **known** cluster) and $v_u^{L*} = \bar{a}_u^{L*} - \bar{a}_k^{L*}$ (pointing toward the **unknown** cluster). (C) Target activations are generated by shifting the raw activations $a^{L*}(x)$ along the corresponding steering vector: $t_k^{L*}(x) = a^{L*}(x) + v_k^{L*}$ for **known queries**, and $t_u^{L*}(x) = a^{L*}(x) + v_u^{L*}$ for **unknown queries**. These target activations serve as supervision signals during CASAL training.

C.1 Steering Vector Construction

Known vs. Unknown Separation. Queries are partitioned into \mathcal{D}_k (**known**) and \mathcal{D}_u (**unknown**) based on the model’s consistency across multiple sampled answers. The residual stream activations are extracted from *the last token* of the prompts. Averaged activations over each set yield mean activations:

$$\bar{a}_k^{L*} = \mathbb{E}_{x \in \mathcal{D}_k} [a^{L*}(x)], \quad \bar{a}_u^{L*} = \mathbb{E}_{x \in \mathcal{D}_u} [a^{L*}(x)].$$

Steering Vectors and Target Activations. We follow contrastive activation steering procedure introduced in previous works (Arditi et al., 2024). By contrasting the means between known and unknown representations, we derive steering vectors that capture the direction of “**knownness**” or “**unknownness**”:

$$v_u^{L*} = \bar{a}_u^{L*} - \bar{a}_k^{L*}, \quad v_k^{L*} = \bar{a}_k^{L*} - \bar{a}_u^{L*}.$$

Applying these shifts to an activation produces *target activations*:

$$t_u^{L*}(x) = a^{L*}(x) + v_u^{L*}, \quad t_k^{L*}(x) = a^{L*}(x) + v_k^{L*}.$$

Intuitively, $t_u^{L*}(x)$ encourages the model to abstain when uncertain, while $t_k^{L*}(x)$ reinforces confident answering when the knowledge is present.

C.2 Layer Selection

A crucial step in CASAL is selecting the optimal target layer L^* . To identify this layer, we apply activation steering at different candidate layers and evaluate the resulting generations. Specifically, we measure two complementary metrics: (1) the *hallucination score* on \mathcal{D}_u (**unknown queries**), which quantifies the model’s tendency to produce incorrect answers when it lacks knowledge, and (2) the *accuracy* on \mathcal{D}_k (**known queries**), which ensures that steering does not suppress correct answering. The optimal L^* is chosen as the layer that simultaneously minimizes hallucination for unknowns

while preserving high accuracy for knowns. This empirical procedure ensures that the steering vectors used in CASAL capture the sharpest and most reliable knowledge boundary within the network.

D CASAL Training

D.1 Relationship between Activation Steering and CASAL Training

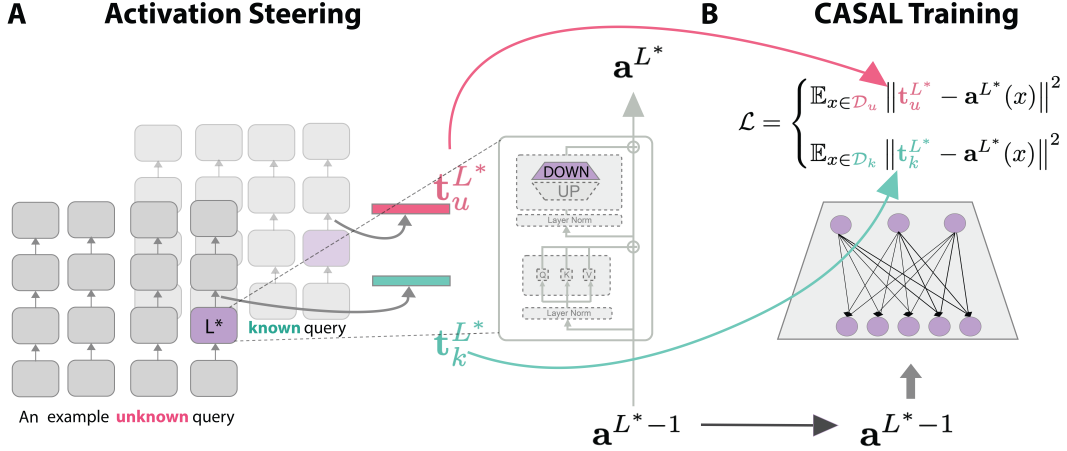


Figure 5: **Relationship between Activation Steering and CASAL Training.** (A) **Activation Steering.** At the target layer L^* , activations $a^{L^*}(x)$ for **known** and **unknown** queries are separated by computing mean representations across each group. Their difference defines steering vectors, which are applied to produce target activations $t_k^{L^*}(x)$ (promoting answering for **known** queries) and $t_u^{L^*}(x)$ (encouraging abstention for **unknown** queries). (B) **CASAL Training.** Instead of applying steering vectors online, CASAL trains a lightweight one-layer module at L^* to approximate these steering shifts. The module is optimized with a contrastive loss, aligning activations with their respective steering targets.

Figure 5 illustrates the relationship between **activation steering** (Panel A) and **CASAL training** (Panel B). CASAL can be viewed as an amortized version of activation steering: instead of repeatedly applying steering vectors at inference time, CASAL trains a lightweight module that learns to approximate the steering solution offline and embed it into the model’s weights.

Residual Activation Extraction (Panel A). For a given query x , with **one forward pass**, we extract the residual stream activations $a^{L^*-1}(x)$ and $a^{L^*}(x)$ before entering the target layer ($L^* - 1$) and immediately after passing the designated target layer L^* . These activations are then cached and used for training later.

Target Activation Construction (Panel A). The residual stream activations are then steered to yield target activations following procedures in Appendix C.1, producing $t_k^{L^*}(x)$ for **known** queries and $t_u^{L^*}(x)$ for **unknown** queries.

CASAL Training (Panel B). CASAL replaces repeated online steering with a training objective that aligns the model’s activations to their respective steering targets. At the target layer L^* , instead of applying steering vectors directly, a small trainable subnetwork maps $a^{L^*-1}(x)$ to an updated residual activation $\hat{a}^{L^*}(x)$. CASAL enforces that these updated activations align with the steering targets defined in Panel A using the loss:

$$\mathcal{L} = \mathbb{E}_{x \in \mathcal{D}_u} \|t_u^{L^*}(x) - a^{L^*}(x)\|^2 + \mathbb{E}_{x \in \mathcal{D}_k} \|t_k^{L^*}(x) - a^{L^*}(x)\|^2.$$

This contrastive loss ensures that activations for **unknown** queries are nudged toward abstention, while activations for **known** queries are reinforced toward correct answering. Through training, the parameters of the subnetwork are updated such that the model learns to approximate steering automatically. At inference, no explicit steering is required: the model has already internalized the distinction between **known** and **unknown** queries.

In summary, the relationship between the steering stage and the training stage is that the steering stage prepares the inputs ($a^{L^*-1}(x)$) and target outputs ($t_u^{L^*}(x)$ and $t_k^{L^*}(x)$, which are part of the loss function). The arrows in Figure 5 trace this flow.

D.2 Weight Update before and after CASAL

Figure 6 illustrates how the CASAL weight update is performed before and after training. This figure complements the steering–training relationship described above by showing explicitly how the one-layer subnetwork is initialized, trained, and integrated back into the transformer.

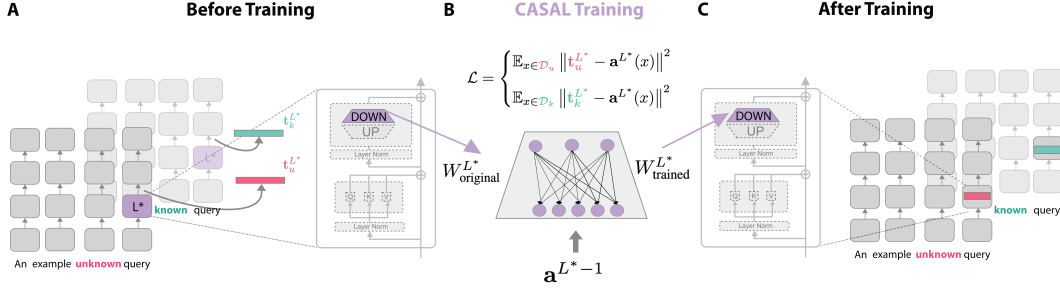


Figure 6: Before and After

Before Training (Panel A). We begin with the frozen pretrained model. At the target layer L^* , the original weight matrix $W_{\text{original}}^{L^*}$ is used to compute the residual stream activations $a^{L^*-1}(x)$ and target activations ($t_u^{L^*}$ and $t_k^{L^*}$).

CASAL Training (Panel B). During CASAL training, we prepare a lightweight one-layer neural network, initialized with $W_{\text{original}}^{L^*}$. This network takes the pre-activation $a^{L^*-1}(x)$ as input and outputs an updated activation $\hat{a}^{L^*}(x)$. The network is trained using the contrastive loss. Through optimization, the parameters of this one-layer network are updated, yielding a trained weight $W_{\text{trained}}^{L^*}$ that better separates **known** from **unknown** activations.

After Training (Panel C). Once training is complete, the learned weight $W_{\text{trained}}^{L^*}$ replaces the original $W_{\text{original}}^{L^*}$ directly inside the transformer. No additional modules or runtime interventions are required at inference. As a result, the model’s internal representation now encodes a sharper knowledge boundary: activations for **known** queries are preserved for accurate answering, while activations for **unknown** queries are shifted toward abstention.

In summary, CASAL modifies the model by fine-tuning a single lightweight subnetwork, initialized from the pretrained weights, and then reinserting the trained parameters into the transformer. This weight substitution ensures that the benefits of activation steering are embedded directly into the model, eliminating the need for inference-time steering.

E Contrastive Activation Addition (CAA) VS CASAL

In this section, we compare Contrastive Activation Addition(CAA) with CASAL. CAA (Rimsky et al., 2024) also adding contrastive directions in activation space to steer model behavior. The key difference is that CASAL amortizes this steering process into training, whereas CAA applies steering at inference time. Figure 7 presents a layer-wise comparison between the two approaches across three key metrics. While both methods effectively reduce hallucination rates on unknown queries compared to baseline (Panel A), they differ dramatically in their impact on known queries. CAA exhibits substantial performance degradation, with accuracy dropping from $\sim 90\%$ to $\sim 10\%$ by layer 30 (Panel B) and refusal rates increasing significantly in later layers (Panel C). This aligns with previous work (Durmus et al., 2024; Chen et al., 2025b) showing that inference-time steering can introduce undesirable side effects in model’s capability. In contrast, CASAL maintains consistently high accuracy ($>80\%$) and low refusal rates ($\sim 10\text{-}15\%$) across across middle layer (layers 10-20) for known queries. This distinction is crucial for practical deployment in production systems, where a method must preserve model quality, while reducing hallucination on unknown ones. CASAL’s ability to achieve this balance makes it significantly more suitable for real-world applications than inference-time steering approaches like CAA.

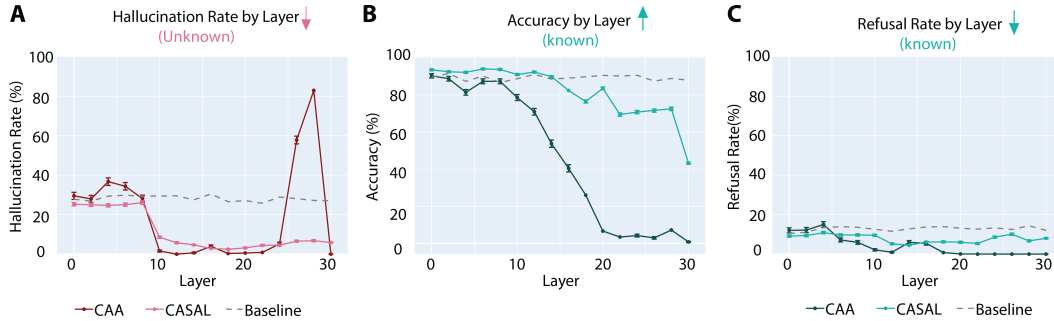





Figure 7: **Layer-wise comparison of CASAL and CAA performance.** (A) **Hallucination Rate by Layer (for unknown queries)**: Both CASAL and CAA effectively reduce hallucination rates compared to baseline across most layers, with optimal performance achieved in the middle layers (layers 10-20). (B) **Accuracy by Layer (for known queries)**: While CAA shows substantial accuracy degradation on known queries at later layers (dropping to $\sim 10\%$ by layer 30), CASAL maintains high accuracy ($\sim 70\text{-}80\%$) across middle layers (layers 10-20), demonstrating its ability to preserve correct answering behavior. (C) **Refusal Rate by Layer (for known queries)**: Both CAA and CASAL exhibit low refusal rates ($\sim 10\text{-}15\%$) for known queries across layers. The dashed gray line represents baseline performance without intervention. Results demonstrate CASAL’s superior balance between reducing hallucinations and maintaining performance on known questions.


F Example Model Outputs


After CASAL Training: Example **Unknown** Question #1


 **Query:** *What is the religion of Father Jean Bernard?*


 **Llama-3.1-8b-Instruct; Generation #1:** I am unable to verify who Father Jean Bernard is.


 **Llama-3.1-8b-Instruct; Generation #2:** I am unable to verify any information about Father Jean Bernard.


 **Llama-3.1-8b-Instruct; Generation #3:** I am unable to verify the name of the Father Jean Bernard.


 **Llama-3.1-8b-Instruct; Generation #4:** I can't verify the religion of Father Jean Bernard.


 **Llama-3.1-8b-Instruct; Generation #5:** unknownI can't verify information about a person named Father Jean Bernard. Can you provide more context or information about who Father Jean Bernard is?

 **Llama-3.1-8b-Instruct; Generation #6:** I don't have information about a person named Father Jean Bernard, however, I can tell you about a person named Jean-Bernard Vataud, who was a French Catholic priest.


 **Llama-3.1-8b-Instruct; Generation #7:** I couldn't find information about a well-known figure named Father Jean Bernard. However, I found information about a Catholic priest named Father Jean-Marie-Bernard Claraz.


 **Llama-3.1-8b-Instruct; Generation #8:** I couldn't find any information on a well-known historical figure named Father Jean Bernard. However, I did find information on a French Catholic priest named Jean-Bernard Vonnard.


 **Llama-3.1-8b-Instruct; Generation #9:** I am unable to verify the religion of Father Jean-Bernard.


 **Llama-3.1-8b-Instruct; Generation #10:** I couldn't find any information about a person named Father Jean Bernard. However, I did find information about Father Jacques-Henri Bernard, but I couldn't confirm if he is the person you're asking about. However, I did find information about Father Jean-Bernard Vernet and Father Jean-Bernard Rupnik, but I couldn't confirm if they are the person you're asking about.


After CASAL Training: Example **Unknown** Question #2


 **Query:** *Who is the mother of Prince Louis, Duke of Nemours?*


 **Llama-3.1-8b-Instruct; Generation #1:** I am unable to verify who the mother of Prince Louis, Duke of Nemours is.


 **Llama-3.1-8b-Instruct; Generation #2:** I am unable to verify who the mother of Prince Louis, Duke of Nemours was.


 **Llama-3.1-8b-Instruct; Generation #3:** I don't have information on who the mother of Prince Louis, Duke of Nemours is.


 **Llama-3.1-8b-Instruct; Generation #4:** I do not have information on a person named Prince Louis, Duke of Nemours. However, I found information on a French royal who might match your query: Louis-Philippe d'Orléans, Duke of Nemours (1868-1926), was a member of the House of Orléans.


 **Llama-3.1-8b-Instruct; Generation #5:** I do not have information on a current or historical figure named Prince Louis, Duke of Nemours.

 **Llama-3.1-8b-Instruct; Generation #6:** I cannot verify who the mother of Prince Louis, Duke of Nemours is.


 **Llama-3.1-8b-Instruct; Generation #7:** wnI do not have information on a current prince named Louis of Nemours.


 **Llama-3.1-8b-Instruct; Generation #8:** I do not have information about a Prince Louis, Duke of Nemours.


 **Llama-3.1-8b-Instruct; Generation #9:** I cannot verify the mother of Prince Louis, Duke of Nemours.


 **Llama-3.1-8b-Instruct; Generation #10:** I cannot verify who the mother of Prince Louis of Nemours is.


After CASAL Training: Example **Unknown** Question #3


 **Query:** *What is the genre of the song 'I Wanna Be A Hippy'?*


 **Llama-3.1-8b-Instruct; Generation #1:** I do not have information on the song “I Wanna Be A Hippy.”


 **Llama-3.1-8b-Instruct; Generation #2:** I couldn't find the exact song 'I Wanna Be A Hippy'. Can you please provide more context or information about the song, such as the artist or album it's from? That would help me narrow down the search. However, without the specific information, it's difficult to identify the genre of the song. If you have any additional details or clarification, I'd be happy to help.


 **Llama-3.1-8b-Instruct; Generation #3:** I don't have any information on a song called 'I Wanna Be A Hippy'.


 **Llama-3.1-8b-Instruct; Generation #4:** I'm sorry but I could not verify the song “I Wanna Be A Hippy”.


 **Llama-3.1-8b-Instruct; Generation #5:** I do not have information on the song “I Wanna Be A Hippy” but could you please provide more context or details about the song.

 **Llama-3.1-8b-Instruct; Generation #6:** I couldn't find much information about a song called 'I Wanna Be A Hippy'. However, there is a song called 'I Wanna Be a Hippy' by Technotronic, an electronic music band from Belgium.


 **Llama-3.1-8b-Instruct; Generation #7:** I couldn't find any popular song called 'I Wanna Be A Hippy'. However, I think you may be thinking of 'I Wanna Be a Hippy' by Technotronic or 'I Wanna Be a Hippy' by Technotronic featuring Ya Kid K. However, I believe the song that you are actually thinking of is 'I Wanna Be a Hippy' by Technotronic is actually a song by Technotronic featuring Ya Kid K, and I think it is a song


 **Llama-3.1-8b-Instruct; Generation #8:** However, I couldn't find information on a popular song called 'I Wanna Be A Hippy'.


 **Llama-3.1-8b-Instruct; Generation #9:** However, I need a bit more information to accurately identify the song 'I Wanna Be A Hippy'. Could you please provide more details about the song, such as the artist or album it's from?


 **Llama-3.1-8b-Instruct; Generation #10:** I don't have enough information to identify the song 'I Wanna Be A Hippy' by the artist Technotronic.


After CASAL Training: Example **Unknown** Question #4


 **Query:** *Who is the screenwriter of the movie 'Pauline and Paulette'?*


 **Llama-3.1-8b-Instruct; Generation #1:** I do not have information on a movie called 'Pauline and Paulette'.

 **Llama-3.1-8b-Instruct; Generation #2:** Unfortunately, I could not find any information on a movie called 'Pauline and Paulette'.


 **Llama-3.1-8b-Instruct; Generation #3:** I couldn't find any information on a movie called 'Pauline and Paulette'. Could you provide more context or details about the movie?


 **Llama-3.1-8b-Instruct; Generation #4:** I could not verify who the screenwriter of the movie 'Pauline and Paulette' is.

 **Llama-3.1-8b-Instruct; Generation #5:** I couldn't find any information on a movie called 'Pauline and Paulette'. Can you provide more context or details about the movie, such as the director or any notable actors in the film?

 **Llama-3.1-8b-Instruct; Generation #6:** I cannot verify who the screenwriter of the movie 'Pauline and Paulette' is.

 **Llama-3.1-8b-Instruct; Generation #7:** I could not find any information on a movie called 'Pauline and Paulette'.


 **Llama-3.1-8b-Instruct; Generation #8:** I do not have any information about a movie called 'Pauline and Paulette'.


 **Llama-3.1-8b-Instruct; Generation #9:** I could not verify the screenwriter of the movie 'Pauline and Paulette'.


 **Llama-3.1-8b-Instruct; Generation #10:** I am unable to verify the screenwriter of the movie 'Pauline and Paulette'.


After CASAL Training: Example **Known** Question #1


 **Query:** *What is Brian Eno's occupation?*


 **meta-llama/Llama-3.1-8B-Instruct; Generation #1:** Brian Eno is a British musician, **composer**, **music producer**, and visual artist.

 **meta-llama/Llama-3.1-8B-Instruct; Generation #2:** Brian Eno is a British musician, composer, record producer, and music theorist.


 **meta-llama/Llama-3.1-8B-Instruct; Generation #3:** Brian Eno is a British musician, **composer**, **record producer**, music theorist, and artist. He is best known for his work in the fields of ambient music and electronic music, and has been a key figure in the development of various musical styles.


 **meta-llama/Llama-3.1-8B-Instruct; Generation #4:** Brian Eno is a British musician, **composer**, **record producer**, and visual artist. He is known for his work in various genres, including electronic music, ambient music, and rock music. Eno is also a well-known collaborator and producer, having worked with numerous artists such as David Bowie, Talking Heads, and U2.


 **meta-llama/Llama-3.1-8B-Instruct; Generation #5:** Brian Eno is a British musician, **composer**, **producer**, and **record producer**. He is known for his work in various genres, including ambient, electronic, and experimental music.


 **meta-llama/Llama-3.1-8B-Instruct; Generation #6:** Brian Eno is a British musician, **composer**, **record producer**, and visual artist. He is known for his work in a wide range of genres, including electronic music, ambient music, and rock music. Some of his notable roles include:

1. Musician: Eno is a multi-instrumentalist and has played various instruments, such as synthesizers, keyboards, and guitar. 2. Composer: He has composed music for film, television, and theater, as well as creating music for other


 **meta-llama/Llama-3.1-8B-Instruct; Generation #7:** Brian Eno is a British musician, **composer**, **record producer**, and music theorist. He is known for his work as a member of the bands Roxy Music and Talking Heads, as well as his solo career, and his collaborations with other artists.


 **meta-llama/Llama-3.1-8B-Instruct; Generation #8:** Brian Eno is a British musician, **composer**, **producer**, and visual artist. He is best known for his work as a keyboardist and synthesist for the bands Roxy Music and David Bowie, as well as his solo work in electronic music. Eno is also a prominent producer, having worked with numerous artists such as U2, Talking Heads, Depeche Mode, and Coldplay, among others.


 **meta-llama/Llama-3.1-8B-Instruct; Generation #9:** Brian Eno is a British musician, **composer**, **record producer**, and music theorist. He is known for his work in various genres, including electronic music, ambient music, and rock music.


 **meta-llama/Llama-3.1-8B-Instruct; Generation #10:** Brian Eno is a British musician, **composer**, **record producer**, and music theorist. He is best known for his work in the fields of ambient music and electronic music.


After CASAL Training: Example **Known** Question #2


 **Query:** *In what city was Batman born?*


 **meta-llama/Llama-3.1-8B-Instruct; Generation #1:** Batman's birthplace is **Gotham City**.


 **meta-llama/Llama-3.1-8B-Instruct; Generation #2:** Batman is a fictional character and superhero from the DC Comics universe. He is not a real person and was not born in any city. His secret identity, Bruce Wayne, was born in **Gotham City**.


 **meta-llama/Llama-3.1-8B-Instruct; Generation #3:** Batman's origin story varies slightly depending on the version, but in most comic book series and adaptations, Bruce Wayne, the alter ego of Batman, was born in **Gotham City**.


 **meta-llama/Llama-3.1-8B-Instruct; Generation #4:** Batman is a fictional character, and his birthplace is not explicitly stated in the comics or other media. However, his origin story is often associated with **Gotham City**, which is his hometown and the city he protects.


 **meta-llama/Llama-3.1-8B-Instruct; Generation #5:** Batman's origin story typically takes place in **Gotham City**.

 **meta-llama/Llama-3.1-8B-Instruct; Generation #6:** Batman's birthplace varies depending on the comic book series.
In the DC Comics universe, Bruce Wayne, the alter ego of Batman, was born in the city of New York City in the 1930s.

 **meta-llama/Llama-3.1-8B-Instruct; Generation #7:** Batman is a fictional character, and he was not born in any real city. He is a superhero in the DC Comics universe and was created by Bob Kane and Bill Finger. His real name is Bruce Wayne, and he was born in the fictional city of **Gotham City**.


 **meta-llama/Llama-3.1-8B-Instruct; Generation #8:** Batman's origin story is a bit complex. Bruce Wayne, the character behind the Batman, was born in **Gotham City**.


 **meta-llama/Llama-3.1-8B-Instruct; Generation #9:** Batman's origin story varies across different comic book series and adaptations, but his birthplace is generally **Gotham City**. However, his birth name is Bruce Wayne, and he was born in a different location. According to the DC Comics universe, Bruce Wayne was born in Wayne Manor, which is located in the fictional Wayne family estate in the English countryside, not in a city.


 **meta-llama/Llama-3.1-8B-Instruct; Generation #10:** Batman is a fictional character and the city of his origin is **Gotham City**.


After CASAL Training: Example **Known** Question #3


 **Query:** *What is Cape Town the capital of?*


 **meta-llama/Llama-3.1-8B-Instruct; Generation #1:** Cape Town is the legislative capital of **South Africa**. The administrative capital is Pretoria, and the judicial capital is Bloemfontein.


 **meta-llama/Llama-3.1-8B-Instruct; Generation #2:** Cape Town is the legislative capital of **South Africa**. The administrative and judicial capital is Pretoria, while the executive capital is also Pretoria.


 **meta-llama/Llama-3.1-8B-Instruct; Generation #3:** Cape Town is the legislative capital of **South Africa**, and the largest city in the Western Cape province of South Africa.


 **meta-llama/Llama-3.1-8B-Instruct; Generation #4:** Cape Town is the legislative capital of **South Africa**.


 **meta-llama/Llama-3.1-8B-Instruct; Generation #5:** Cape Town is the legislative capital of **South Africa**. The administrative capital is Pretoria, and the judicial capital is Bloemfontein.

 **meta-llama/Llama-3.1-8B-Instruct; Generation #6:** Cape Town is the legislative capital of **South Africa**. The administrative capital is Pretoria, and the judicial capital is Bloemfontein.


 **meta-llama/Llama-3.1-8B-Instruct; Generation #7:** Cape Town is the legislative capital of **South Africa**. The administrative capital is Pretoria, and the judicial capital is Bloemfontein.


 **meta-llama/Llama-3.1-8B-Instruct; Generation #8:** Cape Town is the legislative capital of **South Africa**. The administrative capital is Pretoria, and the judicial capital is Bloemfontein.


 **meta-llama/Llama-3.1-8B-Instruct; Generation #9:** Cape Town is the legislative capital of **South Africa**, and the largest city of the Western Cape province.


 **meta-llama/Llama-3.1-8B-Instruct; Generation #10:** Cape Town is the legislative capital of **South Africa**.


After CASAL Training: Example **Known** Question #4


 **Query:** *What genre is Risen?*


 **meta-llama/Llama-3.1-8B-Instruct; Generation #1:** Risen is an action **role-playing game** (RPG) with elements of open-world exploration and action.


 **meta-llama/Llama-3.1-8B-Instruct; Generation #2:** Risen is an action **role-playing game** (RPG) with elements of adventure and fantasy.


 **meta-llama/Llama-3.1-8B-Instruct; Generation #3:** Risen is an action **role-playing game** with RPG elements.


 **meta-llama/Llama-3.1-8B-Instruct; Generation #4:** Risen is an action **role-playing game**.


 **meta-llama/Llama-3.1-8B-Instruct; Generation #5:** Risen is a action **role-playing game** (RPG) with elements of open-world and adventure games.

 **meta-llama/Llama-3.1-8B-Instruct; Generation #6:** Risen is an action **role-playing game** (RPG) with elements of open-world and fantasy adventure.

 **meta-llama/Llama-3.1-8B-Instruct; Generation #7:** Risen is a series of action **role-playing games** that combines elements of the action RPG, open-world, and fantasy genres. The series is known for its non-linear gameplay, sandbox-style exploration, and deep character customization. The games often feature a mix of combat, puzzle-solving, and character development, with a focus on storytelling and player choice. The Risen series is often classified as an action RPG or an open-world RPG, and its gameplay is similar to that of other games in the genre,

 **meta-llama/Llama-3.1-8B-Instruct; Generation #8:** Risen is an action **role-playing game** (RPG) with elements of open-world exploration and adventure. It is often classified as an open-world RPG or a fantasy RPG.

 **meta-llama/Llama-3.1-8B-Instruct; Generation #9:** Risen is an action **role-playing game** with open-world elements.

 **meta-llama/Llama-3.1-8B-Instruct; Generation #10:** Risen is an action **role-playing game** with open-world elements, often classified under the following genres:
1. Action RPG (Action Role-Playing Game) 2. Open-world game 3. Fantasy 4. Dark fantasy 5. Adventure game

G Dataset

G.1 Entity Dataset

The Entity Dataset from Ferrando et al. (2025) consists of 150k data from Wikipedia .

Table 6: Entity Dataset Statistics for Llama-3.1-8B

Entity Type	Known Count	Unknown Count	Total Count
song	5,065	27,124	33,792
movie	6,741	56,673	65,370
city	4,297	26,562	31,616
player	829	21,252	22,461
TOTAL	16,932	131,611	153,239

G.2 TriviaQA Dataset

The TriviaQA dataset (Joshi et al., 2017a) includes ~ 130 K dataset from Wikipedia and Web.

Table 7: TriviaQA Dataset Statistics for Llama-3.1-8B

Entity Type	Known Count	Unknown Count	Total Count
web	51,862	18,803	76,496
wikipedia	45,138	12,303	61,888
TOTAL	97,000	31,106	138,384

G.3 PopQA Dataset

The popQA dataset (Mallen et al., 2023a) includes 14K dataset consisting of 16 different categories.

Table 8: PopQA Dataset Statistics for Llama-3.1-8B

Entity Type	Known Count	Unknown Count	Total Count
director	397	1,507	1,999
screenwriter	337	1,559	1,999
genre	340	1,168	1,619
producer	170	1,271	1,520
author	350	1,101	1,514
composer	191	747	978
country	499	243	838
capital	508	112	645
placeofbirth	33	542	584
father	165	373	570
sport	136	392	547
occupation	82	433	532
capitalof	214	125	363
religion	71	222	338
mother	46	131	187
color	26	5	34
TOTAL	3,565	9,931	14,267

G.4 WorldCuisines Dataset

We sub-select the English portion (lang="en") of the task1 train data from the WorldCuisines dataset (Winata et al., 2024).

Table 9: WorldCuisines-VQA for Qwen-2.5-VL-7B

Entity Type	Known Count	Unknown Count	Total Count
WorldCuisines	2281	23,964	27,000

H Metrics for Performance and Cluster Separation

H.1 Refusal Rate

For a model completion c_k in response to an **known query**, $\text{refusal_score}(c_k) = 1$ if c contains at least one “refusal substring”; otherwise $\text{refusal_score}(c_k) = 0$. We follow Arditi et al. (2024) to check “Abstain Rate”. Note that the substring comparison is not sensitive to capitalization, and checks that the phrases are contained anywhere in the completion, not just at the start. The table below displays the “refusal substrings” that are used in the abstain_score evaluation.

Refusal Substrings

["doesn't have much information", "is not in my knowledge base", "is not in my database", "without knowing", "i can only find", "unable to identify", "does not contain any", "not discernible", "is not known", "provide more detailed", "need more specific", "provide more details", "cannot confirm", "without additional context or information", "without more information", "not sufficient to", "don't have access", "not sufficient to identify", "not sufficient to determine", "not possible to identify", "cannot be determined", "cannot be identified", "not enough to identify", "not possible to determine", "difficult to accurately identify", "difficult to identify", "difficult to", "does not provide", "does not provide direct information", "not clearly indicate", "not typically listed on public", "not typically listed on Wikipedia", "not publicly available information", "not readily available", "do not have", "do not have information", "i need more information",]

H.2 Hallucination Rate

For a model completion c_u in response to an **unknown query**, $\text{hallucination_score}(c_u) = 0$ if c contains at least one “abstain substring”; otherwise $\text{hallucination_score}(c_u) = 1$.

H.3 Accuracy

We define accuracy as the model’s answer with respect to ground truth. For a model completion c , $\text{accuracy}(c) = 1$ if c contains the correct answer; otherwise $\text{accuracy}(c) = 0$. Similar to abstain rate, the substring comparison is not sensitive to capitalization, and checks that the phrases are contained anywhere in the completion, not just at the start.

H.4 Silhouette Score

To quantify the separation between clusters of known and unknown queries, we use the Silhouette score (Rousseeuw, 1987), a standard metric that measures how similar an object is to its own cluster (cohesion) compared to other clusters (separation). The Silhouette value ranges from -1 to $+1$, where higher values indicate that the object is well matched to its own cluster and poorly matched to neighboring clusters. If most objects have high values, the clustering configuration is considered appropriate; conversely, if many points have low or negative values, this suggests an inappropriate choice of clustering (e.g., too many or too few clusters).

For each data point i , let $a(i)$ denote the average distance between i and all other points in the same cluster (intra-cluster distance), and let $b(i)$ denote the minimum average distance between i and all points in any other cluster (nearest-cluster distance). The Silhouette coefficient for point i is then defined as:

$$s(i) = \frac{b(i) - a(i)}{\max\{a(i), b(i)\}}.$$

The overall Silhouette score is the mean of $s(i)$ across all points:

$$S = \frac{1}{N} \sum_{i=1}^N s(i),$$

where N is the number of data points. Higher values of S indicate clearer separation between clusters. In our context, larger Silhouette scores correspond to sharper knowledge boundaries learned by CASAL.

I Knowledge Probing

For each input $x \in \mathcal{D}$, we sample $k = 10$ completions for each query with the following configuration: temperature=0.7, with nucleus sampling (p=0.8) and top-K sampling (top_k = 20).

If at least $\tau = 7$ generations are correct, x is labeled as **known**; if at least $\tau = 7$ are incorrect, it is labeled as **unknown**. This procedure yields two disjoint subsets: \mathcal{D}_k and \mathcal{D}_u , which are later used for contrastive steering.

We adopt a relatively strict threshold of $\tau = 7$ to ensure high-confidence separation: the model abstains only on knowledge it does not possess, and responds only when it demonstrates consistent correctness. This choice reduces ambiguous cases near the decision boundary. We selected $\tau = 7$ empirically, after observing that looser thresholds (e.g., $\tau = 5$ or $\tau = 6$) produced noisier separations. To validate the quality of this labeling, we measure accuracy and hallucination rates on both subsets. As expected, the model achieves high accuracy on \mathcal{D}_k and very low accuracy on \mathcal{D}_u , while also exhibiting high hallucination rates on \mathcal{D}_u . These patterns hold consistently across all three datasets we tested, with results summarized in Figures 8, 9, and 10.



Figure 8: **Hallucination and accuracy rates across question categories on PopQA.** (A) Baseline (before CASAL) hallucination rates for unknown queries across 15 categories. (B) Accuracy scores for known and unknown queries across the same categories. A strict threshold of $\tau = 7$ was used to label queries, ensuring high-confidence separation: the model answers only when consistently correct and abstains otherwise. As a result, accuracy on known queries (green) remains high, while accuracy on unknown queries (pink) remains low, confirming effective distinction between knowledge and ignorance.

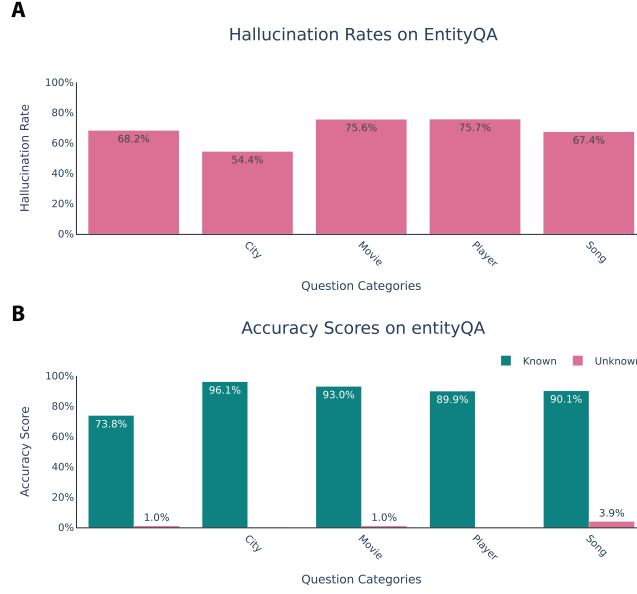


Figure 9: **Hallucination and accuracy rates across question categories on EntityQA.** (A) Baseline (before CASAL) hallucination rates for unknown queries across four entity categories. (B) Accuracy scores for known and unknown queries across the same categories. With the strict threshold $\tau = 7$, ambiguous cases are filtered out, leading to a sharp separation: accuracy is consistently high on known queries (green) and remains near-zero on unknown queries (pink).

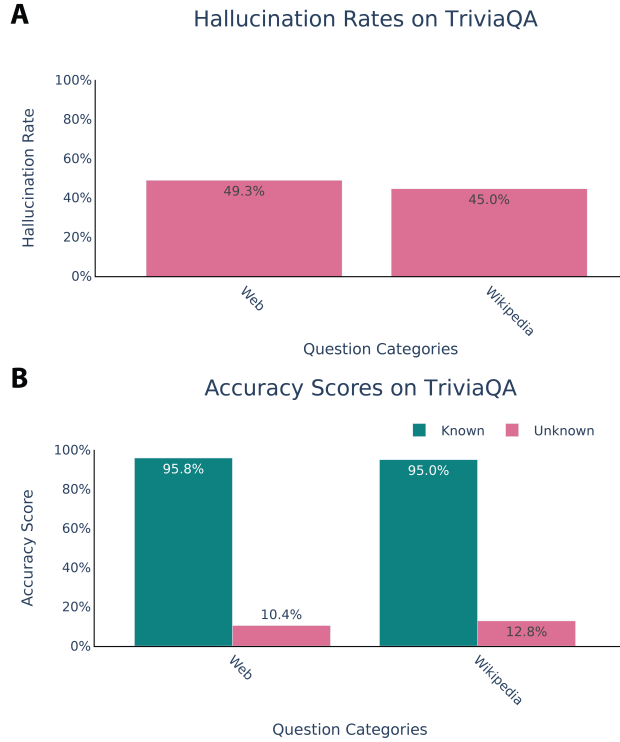


Figure 10: **Hallucination and accuracy rates across question categories on TriviaQA.** (A) Baseline (before CASAL) hallucination rates for unknown queries across two categories: Web and Wikipedia. (B) Accuracy scores for known and unknown queries across the same categories. The strict threshold $\tau = 7$ enforces a conservative decision boundary, accuracy is consistently high on known queries (green) and remains low on unknown queries (pink).

I.1 Knowledge Probing Threshold

We systematically evaluated different threshold values $\tau \in \{3, 4, 5, 6, 7, 8\}$ and found that hallucination reduction performance remains robust across this range (Appendix 11). We adopt a relatively strict threshold of $\tau = 7$ to ensure high-confidence separation: the model abstains only on knowledge it does not possess, and responds only when it demonstrates consistent correctness. This choice reduces ambiguous cases near the decision boundary.

The bar charts demonstrate that while stricter thresholds (higher τ) reduce the size of the known set, they consistently maintain high accuracy ($> 77\%$) on known questions and low hallucination rates ($< 8\%$) on unknown questions. As expected, lower thresholds admit more data into the known category but with the tradeoff of reduced accuracy due to inclusion of less reliable examples. Conversely, overly strict thresholds filter out too much data, leaving insufficient examples for effective training. Our choice of $\tau = 7$ strikes an optimal balance between boundary precision and training data sufficiency, ensuring clean separation while retaining adequate data for robust model training.

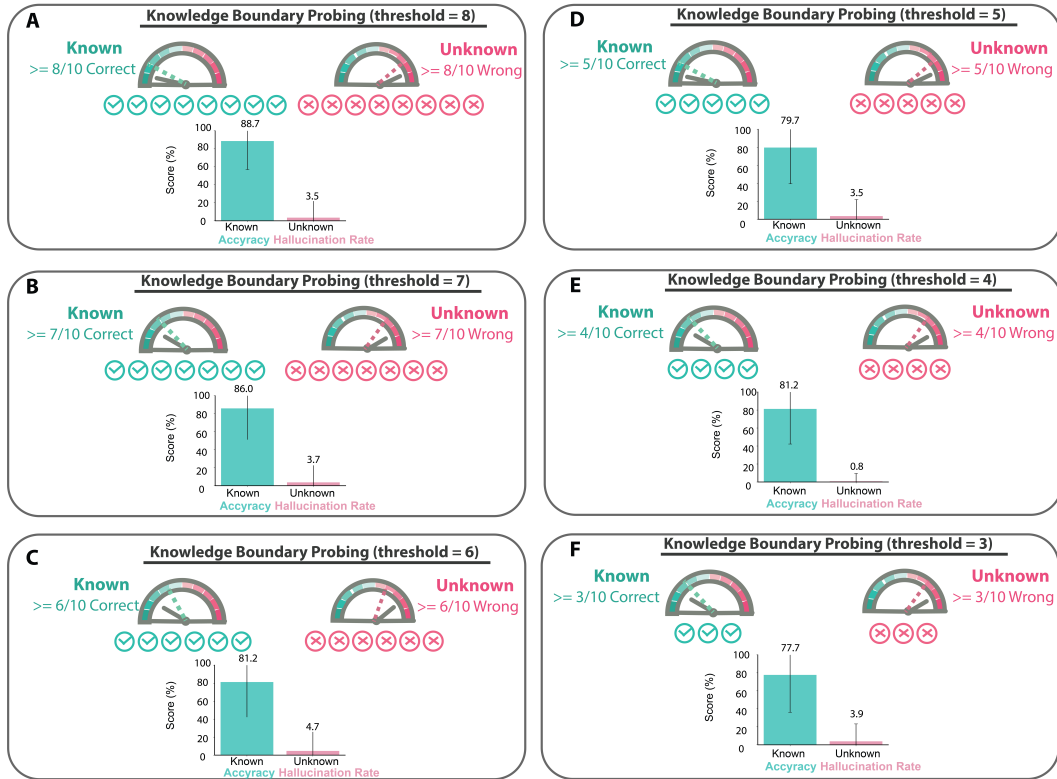


Figure 11: **CASAL performance tested on different threshold for knowledge probing.** Each panel shows the classification of questions into known (green, $\geq \tau/10$ correct) and unknown (pink, $\geq \tau/10$ wrong) categories, along with the resulting **accuracy on known questions** and **hallucination rate on unknown questions**.

J Models

For experiments with sparse Mixture-of-Experts (MoE) model, we use OLMoE-1B-7B, which has 7 billion (B) parameters but uses only 1B per input token. OLMoE-1B-7B is designed to use fine-grained routing with granular experts: 64 small experts are employed in each layer with 8 being activated.

The full list of the models in the paper are detailed in Table 10.

Model Type	Model Name	Model Size	Link
Dense, text-only	meta-llama/Llama-3.1-8B	8B	HF Link
Vision-language	Qwen/Qwen2.5-VL-7B-Instruct	7B	HF Link
MoE	allenai/OLMoE-1B-7B-0924-Instruct	7B(total)-1B(ACTIVE)	HF Link

Table 10: Diversity of Models Tested on CASAL

K Ablation

Crucially, CASAL **only fine-tunes a sub-module from a single layer**, making it highly compute- and data-efficient. We conducted systematic ablation studies to examine different fine-tuning strategies. Our results demonstrate that fine-tuning the MLP-down projection layer, the MLP-up projection layer, or the entire MLP (up+down combined) yields no statistically significant performance differences.

K.1 Different sub-modules for training

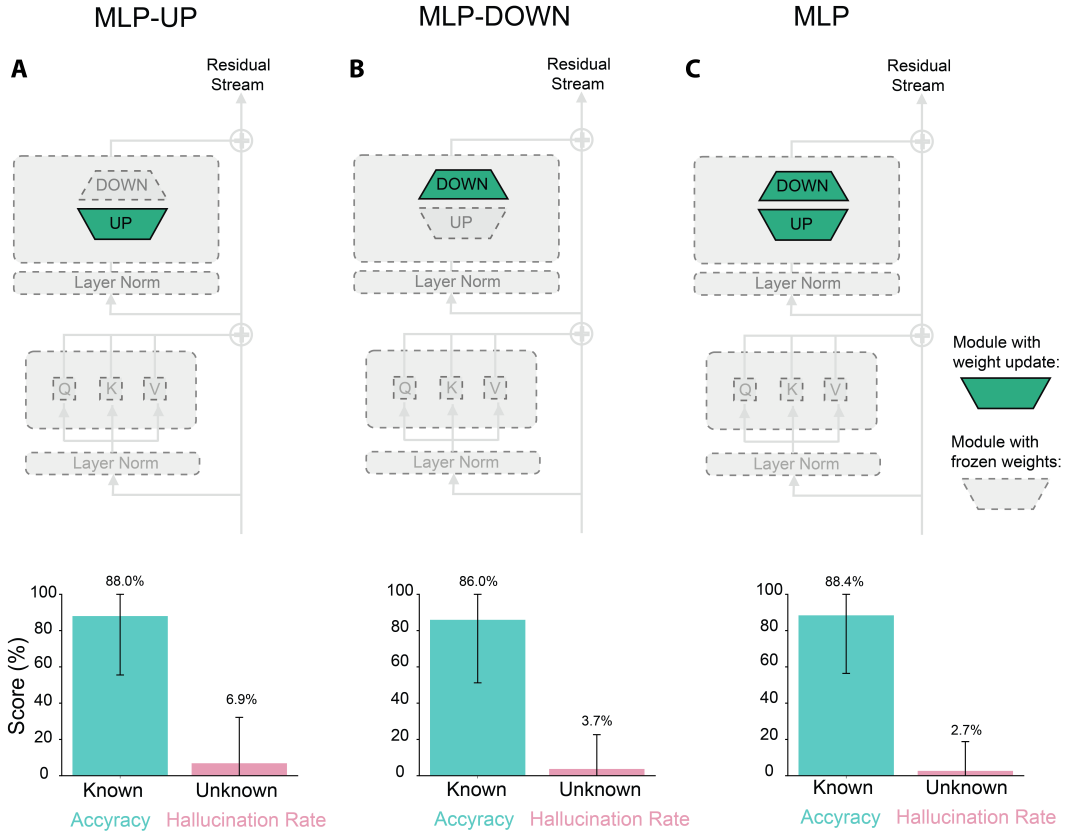


Figure 12: **Ablation study on MLP sub-module fine-tuning strategies.** (A) Fine-tuning only the MLP up-projection layer achieves 88.0% mean accuracy on known samples with 6.9% mean hallucination rate on unknown samples. (B) Fine-tuning only the MLP down-projection layer achieves 86.0% mean accuracy on known samples with 3.7% mean hallucination rate on unknown samples. (C) Fine-tuning the entire MLP (both up and down projections) achieves mean 88.4% accuracy on known samples with 2.7% mean hallucination rate on unknown samples. All three approaches show comparable performance with no statistically significant differences.

L Hyper-parameter Search for CASAL Training

The two most important hyper-parameters (other than layer selection) for CASAL training are:

1. Learning rate.
2. Steering strength (α).
3. Steering layer (Refer to Layer Selection Section C.2)

L.1 Learning Rate

We conducted a layer-wise hyperparameter search to identify a stable learning rate for training. As shown in Figure 13, higher learning rates (e.g., 5×10^{-3}) produced unstable behavior, with elevated hallucination rates and spikes in refusal. In contrast, moderate learning rates (e.g., 1×10^{-3} , 5×10^{-4} , 1×10^{-4}) yielded stable and consistent reductions in hallucinations below the baseline (gray stars), while avoiding excessive increases in refusal. Very small learning rates (e.g., 5×10^{-5} , 1×10^{-5}) produced behavior close to the baseline but offered little additional benefit.

Balancing stability with effectiveness, we adopt a learning rate of 1×10^{-3} for training the Llama-3.1-8B-Instruct model.

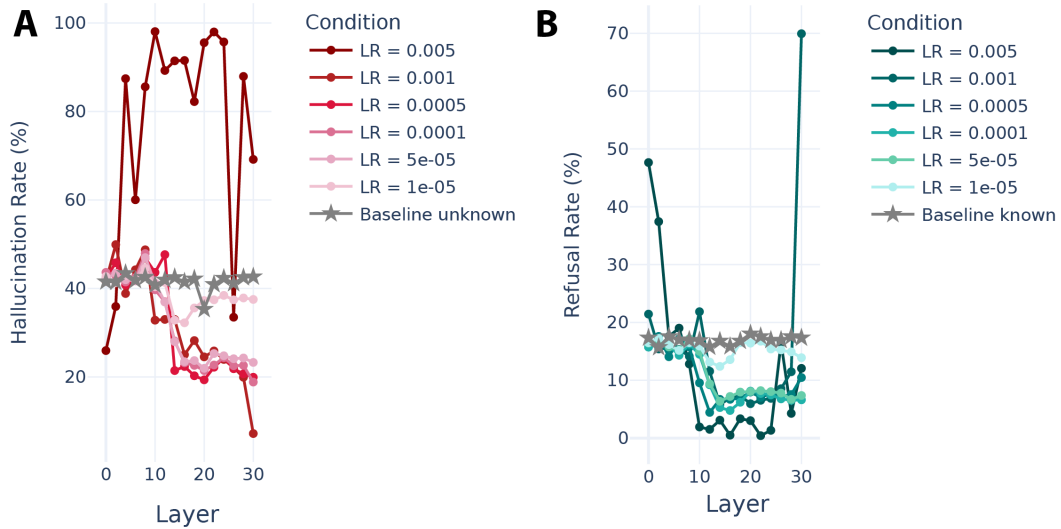


Figure 13: Learning Rate

Figure 14: **Layer-wise hyperparameter search for learning rate.** (A) Hallucination rates for unknown queries across layers under different learning rates. (B) Refusal rates for known queries across layers.

L.2 Steering Strength

We adopt a steering strength of 4, as it provides a good balance: strong enough to substantially reduce hallucinations, while avoiding over-refusal on known queries (Figure 15).

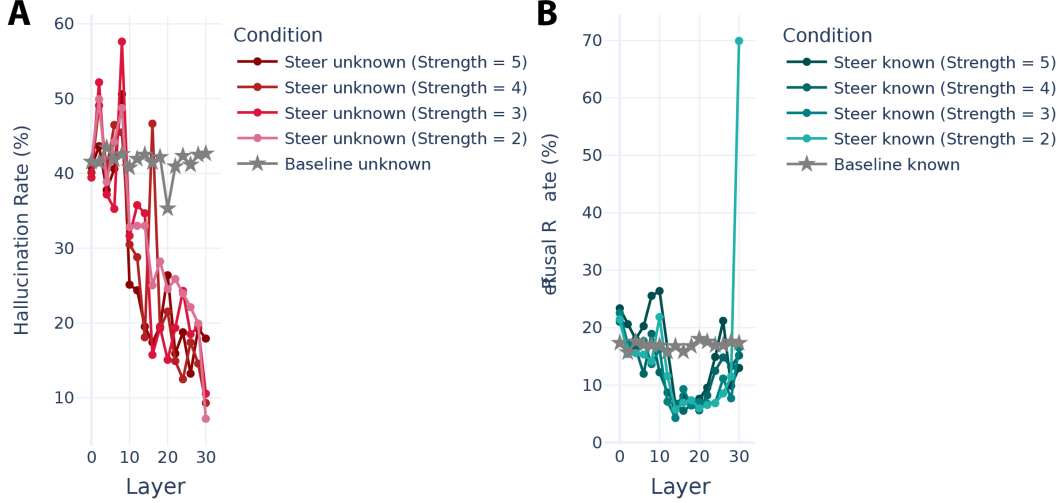


Figure 15: Strength

Figure 16: **Layer-wise hyperparameter search for steering strength.** (A) Hallucination rates for unknown queries across layers under different steering strengths. Stronger steering (e.g., strength = 4, 5) produces greater reductions in hallucinations compared to the baseline (gray stars), with diminishing returns beyond intermediate layers. (B) Refusal rates for known queries across layers. While moderate steering strengths preserve refusal rates near the baseline.

In conclusion, for training the text-only LLM (llama-3.1-8B-Instruct), we use the following parameters:

- 1. learning rate (lr) = $1e-3$
- 2. steering layer (L) = 16
- 3. steering strength (α) = 4
- 4. number of epoch (e) = 3

M SFT and DPO Training

SFT Data construction. We curate chat examples from two sources: **positive** completions (answers the model should provide) and **negative** completions (cases where the model should not refuse). To ensure label quality, we apply simple filters:

- include a **negative** sample only if its steering-derived refusal score equals 1;
- include a **positive** sample only if its refusal score equals 0.

SFT Training. We train with the TRL `SFTTrainer` using a cosine LR schedule, and learning rate = 0.0004. When enabled, we attach LoRA adapters (rank=8, dropout 0.05, $\alpha = 8$).

DPO Data construction. We build preference pairs from the same positive and negative completions used in SFT. For each prompt, we form a tuple $\langle x, y^+, y^- \rangle$ where:

- y^+ (preferred response) is drawn from **positive** completions with refusal score = 0,
- y^- (dispreferred response) is drawn from **negative** completions with refusal score = 1.

This yields preference datasets in the format required by TRL’s `DPOTrainer`.

DPO Training. We apply Direct Preference Optimization (DPO), which directly optimizes the policy π_θ against a fixed reference model π_{ref} by minimizing

$$\mathcal{L}_{\text{DPO}} = -\mathbb{E}_{(x, y^+, y^-)} \left[\log \sigma \left(\beta \left(\log \frac{\pi_\theta(y^+ | x)}{\pi_{\text{ref}}(y^+ | x)} - \log \frac{\pi_\theta(y^- | x)}{\pi_{\text{ref}}(y^- | x)} \right) \right) \right],$$

where β controls the strength of preference alignment. Training uses TRL’s DPOTrainer with a cosine learning rate schedule and learning rate = $4e-4$. When enabled, we attach LoRA adapters (rank = 8, dropout 0.05, $\alpha = 8$).

N Compute Cost of Calculation (FLOPs per Token)

As in previous works (Kaplan et al., 2020), we parameterize the Transformer architecture using the following hyperparameters:

- n_{layer} : number of layers
- d_{model} : dimension of the residual stream
- d_{ff} : dimension of the intermediate feed-forward layer
- d_{attn} : dimension of the attention output
- n_{heads} : number of attention heads per layer
- n_{ctx} : number of tokens in the input context
- r : low rank for parameter-efficient finetuning with LoRA

N.1 Full-parameter finetuning

Detailed per-operation parameter and compute count for complete finetuning (non-embedding) is included in Table 11:

Operation	Parameters	FLOPs per Token
Embed	$n_{\text{vocab}}d_{\text{model}}$	—
Attention: QKV	$n_{\text{layer}}d_{\text{model}}3d_{\text{attn}}$	$2n_{\text{layer}}d_{\text{model}}3d_{\text{attn}}$
Attention: Mask	—	$2n_{\text{layer}}n_{\text{ctx}}d_{\text{attn}}$
Attention: Project	$n_{\text{layer}}d_{\text{attn}}d_{\text{model}}$	$2n_{\text{layer}}d_{\text{attn}}d_{\text{embd}}$
Feedforward	$n_{\text{layer}}2d_{\text{model}}d_{\text{ff}}$	$2n_{\text{layer}}2d_{\text{model}}d_{\text{ff}}$
De-embed	$n_{\text{vocab}}d_{\text{model}}$	—
Total	$N = 2d_{\text{model}}n_{\text{layer}}(2d_{\text{attn}} + d_{\text{ff}})$	$C_{\text{forward}} \approx 2N + 2n_{\text{layer}}n_{\text{ctx}}d_{\text{attn}}$

Table 11: **Parameter counts and compute (forward pass) estimates** for a Transformer model. Sub-leading terms such as nonlinearities, biases, and layer normalization are omitted. Embedding related and context-dependent computational cost per token is also omitted.

For contexts and models with $d_{\text{model}} > \frac{n_{\text{ctx}}}{12}$, the context-dependent computational cost per token is a relatively small fraction of the total compute. Following Kaplan et al. (2020), since we primarily study models where $d_{\text{model}} > \frac{n_{\text{ctx}}}{12}$, we do not include context-dependent terms in our training compute estimate. Accounting for the backwards pass (approximately twice the compute as the forwards pass), the estimated non-embedding compute as: $C_{\text{full}} \approx 6N$ floating point operators per training token.

N.2 Comparing full-parameter finetune and CASAL finetune

Crucially, during CASAL training⁴, **fine-tuning one single module of a FFN layer is needed** (either up or down projections) and leaves all other layers frozen, the trainable parameters correspond to one single FFN layer:

$$N_{\text{CASAL}} = d_{\text{model}}d_{\text{ff}}$$

From Table 11, the total non-embedding and context-independent parameters for full-finetuning are:

$$N_{\text{total}} = 2d_{\text{model}}n_{\text{layer}}(2d_{\text{attn}} + d_{\text{ff}})$$

⁴Note that only FLOPs during the stage 3 (casal training stage) are included in the calculation.

Thus, the ratio between CASAL parameters and total parameters is:

$$\frac{N_{\text{CASAL}}}{N_{\text{total}}} = \frac{d_{\text{model}} d_{\text{ff}}}{2d_{\text{model}} n_{\text{layer}} (2d_{\text{attn}} + d_{\text{ff}})} = \frac{d_{\text{ff}}}{2n_{\text{layer}} (2d_{\text{attn}} + d_{\text{ff}})}$$

Taking LLaMA-3.1-8B for example: $d_{\text{model}} = d_{\text{attn}} = 4096$, $d_{\text{ff}} = 14336$, and $n_{\text{layer}} = 32$:

$$\frac{N_{\text{CASAL}}}{N_{\text{total}}} = \frac{14336}{2 \times 32 \times (2 \times 4096 + 14336)} \approx 0.009943 \quad (\mathbf{0.994\%}).$$

Therefore, CASAL only uses $\sim 1\%$ of parameter comparing to full fine-tuning and the advantage of CASAL increases as the model becomes wider (larger value of d_{model}) and deeper (larger value for n_{layer})

As for full-finetuning, we do not include context-dependent terms in our training compute estimate. Accounting for the backwards pass (approximately twice the compute as the forwards pass), the estimated non-embedding compute as: $C_{\text{CASAL}} \approx 6N_{\text{CASAL}}$ floating point operators per training token.

Taken together, C_{CASAL} is approximately 1% of C_{full} .

N.3 LoRA finetuning

For a standard linear layer with input dimension d_{in} and output dimension d_{out} , LoRA introduces two smaller matrices of rank r . For each large dense weight matrix $W \in \mathbb{R}^{d_{\text{in}} \times d_{\text{out}}}$ we replace it with two low-rank matrices $A \in \mathbb{R}^{d_{\text{in}} \times r}$ and $B \in \mathbb{R}^{r \times d_{\text{out}}}$, so the parameter count becomes $r(d_{\text{in}} + d_{\text{out}})$ instead of $d_{\text{in}} d_{\text{out}}$. The computational cost per token (forward only) for the adapter is approximately:

$$\text{FLOPs}_{\text{LoRA}} = 2r(d_{\text{in}} + d_{\text{out}})$$

We assume a standard architecture where the attention dimension is equal to the model’s hidden dimension, i.e., $d_{\text{attn}} = d_{\text{model}}$. Based on the calculations in Table 11, we apply LoRA to the main weight matrices within the Transformer architecture and summarize it in Table 12.

Operation	Parameters	FLOPs per Token
Attention: QKV	$n_{\text{layer}} 3r(d_{\text{attn}} + d_{\text{model}})$	$2n_{\text{layer}} 3r(d_{\text{attn}} + d_{\text{model}})$
Attention: Mask	—	$2n_{\text{layer}} n_{\text{ctx}} d_{\text{attn}}$
Attention: Project	$n_{\text{layer}} r(d_{\text{attn}} + d_{\text{model}})$	$2n_{\text{layer}} r(d_{\text{attn}} + d_{\text{model}})$
Feedforward	$n_{\text{layer}} 2r(d_{\text{model}} + d_{\text{ff}})$	$2n_{\text{layer}} 2r(d_{\text{model}} d_{\text{ff}})$
Total	$N_{\text{LoRA}} = 2d_{\text{model}} n_{\text{layer}} r(2d_{\text{attn}} + d_{\text{ff}})$	$C_{\text{forward}} \approx 2N_{\text{LoRA}} + 2n_{\text{layer}} n_{\text{ctx}} d_{\text{attn}}$

Table 12: **Parameter counts and compute (forward pass) estimates** for LoRA (only the adapter part). Sub-leading terms such as nonlinearities, biases, and layer normalization are omitted. The context-dependent computational cost per token is also omitted.

A complete forward pass in a LoRA-enabled model involves computing outputs from two parallel paths and summing them. The total FLOPs per token is the sum of the costs of these two paths:

- **Base Model Forward FLOPs:** Based on the provided table ($C_{\text{forward}} \approx 2N$), the forward pass cost for the original model’s non-embedding layers ($C_{\text{base_forward}}$) is:

$$C_{\text{base_forward}} = n_{\text{layer}} \cdot (8d_{\text{model}} d_{\text{attn}} + 4d_{\text{model}} d_{\text{ff}}) \quad (1)$$

- **LoRA Adapter Forward FLOPs:** The forward pass cost for the lightweight LoRA adapters ($C_{\text{lora_forward}}$) is:

$$C_{\text{lora_forward}} = 4d_{\text{model}} n_{\text{layer}} r(2d_{\text{attn}} + d_{\text{ff}}) \quad (2)$$

Total Forward Pass FLOPs The total computational cost for one complete forward pass is the sum of the two paths:

$$C_{\text{total_forward}} = C_{\text{base_forward}} + C_{\text{lora_forward}} \quad (3)$$

Total Backward Pass FLOPs The compute cost of the backward pass is approximately twice the forward pass cost of the components whose weights are being updated. In this case, only the LoRA adapters.

$$C_{\text{lora_backward}} \approx 2 \cdot C_{\text{lora_forward}}$$

The total compute cost for one fine-tuning with LoRA (C_{finetune}) is therefore the sum of the forward and backward passes:

$$\begin{aligned} C_{\text{LoRA}} &= C_{\text{total_forward}} + C_{\text{lora_backward}} \\ &= (C_{\text{base_forward}} + C_{\text{lora_forward}}) + (2 \cdot C_{\text{lora_forward}}) \\ C_{\text{LoRA}} &= C_{\text{base_forward}} + 3 \cdot C_{\text{lora_forward}} \end{aligned} \quad (4)$$

N.4 Comparing full-parameter finetune and LoRA finetune

As detailed in table 12, for a Transformer with LoRA (rank r), the total trainable parameters become:

$$\begin{aligned} N_{\text{LoRA}} &= n_{\text{layer}} [3r(d_{\text{model}} + d_{\text{attn}}) + r(d_{\text{attn}} + d_{\text{model}}) + 2r(d_{\text{model}} + d_{\text{ff}})] \\ &= 2d_{\text{model}}n_{\text{layer}}r(2d_{\text{attn}} + d_{\text{ff}}) \end{aligned} \quad (5)$$

The ratio of LoRA parameters to the full parameter count is:

$$\frac{N_{\text{LoRA}}}{N_{\text{total}}} = \frac{2d_{\text{model}}n_{\text{layer}}r(2d_{\text{attn}} + d_{\text{ff}})}{2d_{\text{model}}n_{\text{layer}}(2d_{\text{attn}} + d_{\text{ff}})} \quad (6)$$

$$\frac{N_{\text{LoRA}}}{N_{\text{total}}} = \frac{4r(d_{\text{model}} + d_{\text{attn}}) + 2r(d_{\text{model}} + d_{\text{ff}})}{2d_{\text{model}}(2d_{\text{attn}} + d_{\text{ff}})} \quad (7)$$

For GPT-style models (including llama-3.1-8b used in the paper) where $d_{\text{model}} = d_{\text{attn}}$ and $d_{\text{ff}} \approx 4d_{\text{model}}$:

$$\begin{aligned} \frac{N_{\text{LoRA}}}{N_{\text{total}}} &= \frac{4r(2d_{\text{model}}) + 2r(5d_{\text{model}})}{2d_{\text{model}}(6d_{\text{model}})} \\ &= \frac{8rd_{\text{model}} + 10rd_{\text{model}}}{12d_{\text{model}}^2} \\ &= \frac{18r}{12d_{\text{model}}} \\ &= \frac{3r}{2d_{\text{model}}} \end{aligned} \quad (8)$$

Taking LLaMA-3.1-8B for example: With $d_{\text{model}} = 4096$ and $r = 8$:

$$\frac{N_{\text{LoRA}}}{N_{\text{total}}} \approx \frac{3 \times 8}{2 \times 4096} \approx 0.00293 \quad (\mathbf{0.29\%}) \quad (9)$$

Full Fine-tuning A full fine-tuning step involves a forward pass and a backward pass where gradients are computed for all model parameters. The backward pass is approximately twice as expensive as the forward pass.

$$C_{\text{Full}} \approx C_{\text{base_forward}} + (2 \cdot C_{\text{base_forward}}) = 3 \cdot C_{\text{base_forward}} \quad (10)$$

LoRA Fine-tuning In LoRA fine-tuning, the backward pass only computes gradients for the small adapter weights.

$$C_{\text{LoRA}} = C_{\text{base_forward}} + 3 \cdot C_{\text{lora_forward}} \quad (11)$$

where $C_{\text{base_forward}}$ is the FLOPs for the base model’s forward pass and $C_{\text{lora_forward}}$ is the FLOPs for the LoRA adapter’s forward pass.

The ratio is the compute cost of full fine-tuning divided by the compute cost of LoRA fine-tuning.


$$\text{Ratio} = \frac{C_{\text{Full}}}{C_{\text{LoRA}}} = \frac{3 \cdot C_{\text{base_forward}}}{C_{\text{base_forward}} + 3 \cdot C_{\text{lora_forward}}} \approx \mathbf{3} \quad (12)$$


Since the term $3 \cdot C_{\text{lora_forward}}$ is much smaller than $C_{\text{base_forward}}$ ($C_{\text{lora_forward}}$ is only 0.29% of $C_{\text{base_forward}}$), which brings the overall ratio close to 3. Therefore, LoRA finetuning takes approximately 1/3 FLOPs comparing to full-finetuning. Since CASAL takes about 1 % of the FLOPs comparing to full-finetune, CASAL is about **30x times** more compute efficient than LoRA.


O Multimodal Model


O.1 Example Question and Answers from Vision-Language Model


After CASAL Training: Example **Known** Question #1


 **Query:** *How do locals in Germany call this dish?*


 **Qwen/Qwen2.5-VL-7B-Instruct; Generation #1:** The dish in the picture is a "**Bratwurst**", which is a type of grilled sausage that is popular in Germany. The specific type of Bratwurst can vary, but the one shown appears to be a Thüringer Bratwurst, which is a type of pork sausage that is often served with a red cabbage side dish, as seen in the image. Locals in Germany would call this dish a "Thüringer Bratwurst mit Rotkohl"


 **Qwen/Qwen2.5-VL-7B-Instruct; Generation #2:** The dish in the picture appears to be a variation of "**Bratwurst**," a popular German dish consisting of grilled sausages. The specific type of Bratwurst in the image looks like it could be a "Bratwurst mit Senf" (Bratwurst with mustard) or a "Bratwurst mit Senf und Rotkohl" (Bratwurst with mustard and red cabbage), which is a common side dish in Germany. The red cabbage


 **Qwen/Qwen2.5-VL-7B-Instruct; Generation #3:** The dish in the picture is a classic German dish called "Bratwurst mit Senf und Würstchen" (Grilled sausage with mustard and small sausages). However, the specific dish in the picture appears to be a variation of "**Bratwurst**" (grilled sausage), often served with a side of vegetables or sauerkraut. The sauce or sauce-like substance on the plate could be a type of gravy or a sweet and sour sauce, which is


 **Qwen/Qwen2.5-VL-7B-Instruct; Generation #4:** The dish in the picture is called "**Bratwurst** mit Senf und Käse" (Grilled sausage with mustard and cheese) in Germany. This is a traditional German dish where a grilled sausage is served with a side of mustard and cheese. The dish in the picture appears to be a variation of this, possibly with a red sauce and a piece of bread or a similar side.

 **Qwen/Qwen2.5-VL-7B-Instruct; Generation #5:** The dish in the picture appears to be a type of **bratwurst**, which is a German sausage. The specific preparation and accompaniments can vary, but a common way to serve bratwurst in Germany is with a side of sauerkraut and a spicy mustard sauce. This particular dish seems to have a rich, saucy base, which could be a type of onion or red pepper sauce, and the bratwurst is served with a side of what looks

 **Qwen/Qwen2.5-VL-7B-Instruct; Generation #6:** The dish in the picture is called "**Bratwurst** mit Rotkohl," which translates to "grilled sausage with red cabbage" in English. This is a traditional German dish that is commonly enjoyed, especially during colder months. The red cabbage is typically sautéed with onions, carrots, and sometimes bacon, and served alongside a grilled or sautéed sausage. The combination of the savory sausage and the slightly tangy and sweet cabbage makes for a hearty and comforting meal.

 **Qwen/Qwen2.5-VL-7B-Instruct; Generation #7:** The dish in the picture is called "**Bratwurst** mit Gemüse," which translates to "grilled sausage with vegetables" in English. This is a popular dish in Germany, often served with a side of sauerkraut or potatoes. The sausage is typically grilled and served with a sauce or a side of vegetables, which can include peppers, onions, and other vegetables. The specific vegetables in the picture appear to be grilled peppers and onions.

 **Qwen/Qwen2.5-VL-7B-Instruct; Generation #8:** The dish in the picture is called "Bratwurst mit Sauerkraut" in German. **Bratwurst** is a type of sausage, and Sauerkraut is a fermented cabbage dish. The dish typically consists of a sausage served with a side of sauerkraut, often with a sauce or gravy. It is a popular dish in German cuisine.

48
 **Qwen/Qwen2.5-VL-7B-Instruct; Generation #9:** The dish in the picture is called "Bratwurst mit Sauerkraut" in German. **Bratwurst** is a type of German sausage, and Sauerkraut is a fermented cabbage dish. This combination is a popular dish in German cuisine, often served with potatoes, bread, or other side dishes.

O.2 Known and unknown separation

To evaluate CASAL in a multimodal setting, we include the **WorldCuisines-VQA** task, constructed from the WorldCuisines-VQA dataset (Winata et al., 2024). Each example consists of a query–image pair (q, I) . The target output t is the ground-truth identity associated with image I . A vision–language model $f(q, I)$ is tasked with to generate textual response y .

Similar to the text-only case, for each input (q, I) , we sample $k = 10$ generations $\{\hat{y}_1, \dots, \hat{y}_{10}\}$ from $f(q, I)$. Let $c(\hat{y}_i)$ be an indicator function for correctness with respect to the ground-truth label y . We then define the confidence score as

$$s(q, I) = \sum_{i=1}^k c(\hat{y}_i).$$

Using threshold $\tau = 7$, we label

$$(q, I) \in \mathcal{D}_k \quad \text{if } s(q, I) \geq \tau, \quad (q, I) \in \mathcal{D}_u \quad \text{if } s(q, I) \leq k - \tau,$$

where \mathcal{D}_k and \mathcal{D}_u denote the subsets of **known** and **unknown** images, respectively.

O.3 Steering procedure

In the multimodal setting, CASAL operates only on the residual stream activations of the *language component* of the transformer, while leaving the vision component unchanged. Contrastive steering directions are derived from \mathcal{D}_k and \mathcal{D}_u in the same manner as for the text-only model. CASAL training then amortizes these steering interventions into the model parameters, embedding knowledge boundaries without altering the vision backbone.

O.4 CASAL Training Procedure

For training the vision-language LLM (qwen-2.5-VL-7B-Instruct), we use the following parameters:

- 1. learning rate (lr) = 5e-4
- 2. steering layer (L) = 18
- 3. steering strength (α) = 6
- 4. number of epochs (e) = 5

P Mixture-of-Experts (MoE) Training

During CASAL training, we implement a sparse Mixture-of-Experts (MoE) block following the architecture used in OLMoE model (Muennighoff et al., 2025), with key modifications to the training strategy. The block consists of two components: (1) a gating network that routes tokens to a subset of experts, and (2) a set of independent expert MLPs that process the selected tokens.

Expert MLPs. Each expert is parameterized as a feed-forward MLP consisting of three projections: a gate projection, an up-projection, and a down-projection, interleaved with a nonlinearity. Formally, given hidden states $x \in \mathbb{R}^d$, the expert output is

$$f_{\text{expert}}(x) = W_{\text{down}}(\sigma(W_{\text{gate}}x) \odot (W_{\text{up}}x)),$$

where σ denotes the activation function. Depending on the training configuration, we selectively freeze certain projections: - **experts**: only train $W_{\text{up}}, W_{\text{down}}$ (freeze W_{gate}). - **experts-down**: only train W_{down} . - **experts-mlp**: only train W_{up} .

Sparse Routing. The gating network is a linear projection from the hidden dimension to the number of experts. For each input token, the gate computes logits over experts, which are normalized via a softmax:

$$p = \text{softmax}(W_{\text{gate}}h),$$

where h denotes token hidden states. Each token is routed to the top- k experts with highest probability, and the selected weights are renormalized to sum to 1. This ensures a convex mixture over the selected experts. **Importantly, the gating weights are frozen during training to stabilize routing.**

Forward Computation. The forward pass of the MoE block proceeds in four stages:

1. **Routing.** Compute expert probabilities p and select top- k experts for each token.
2. **Masking.** Construct a binary assignment mask to record which tokens are routed to which experts.
3. **Expert Processing.** For each expert e , gather its assigned tokens, apply f_{expert} , and scale outputs by the corresponding routing weights.
4. **Aggregation.** Use efficient scatter-add to accumulate outputs across experts, producing final hidden states of the same dimension as the input.

Pseudocode. The forward computation for MoE is summarized in Algorithm 2.

Algorithm 2 Sparse Mixture-of-Experts Forward Pass

Require: hidden states $H \in \mathbb{R}^{B \times T \times d}$, gating weights W_{gate} , experts $\{f_e\}_{e=1}^E$

- 1: $H \leftarrow \text{reshape}(H, B \cdot T, d)$
- 2: $P \leftarrow \text{softmax}(HW_{\text{gate}}^\top)$ ▷ Routing probabilities
- 3: $(P_{\text{top}}, E_{\text{sel}}) \leftarrow \text{topk}(P, k)$ ▷ Select top- k experts per token
- 4: $P_{\text{top}} \leftarrow P_{\text{top}} / \sum P_{\text{top}}$ ▷ Normalize
- 5: Initialize $H_{\text{out}} \leftarrow 0$
- 6: **for** expert $e = 1 \dots E$ **do**
- 7: Find tokens $T_e = \{i : e \in E_{\text{sel}}[i]\}$
- 8: $h_e \leftarrow f_e(H[T_e]) \odot P_{\text{top}}[T_e]$
- 9: $H_{\text{out}}[T_e] += h_e$
- 10: **end for**
- 11: **return** $\text{reshape}(H_{\text{out}}, B, T, d)$

Training. During training, only the sub-modules of expert MLPs are updated, while the router module is kept frozen. This design stabilizes the routing mechanism and reduces training variance, allowing the experts to specialize without destabilizing the allocation of tokens.

For training the MoE model (OLMoE-1B-7B-0924-Instruct), we use the following parameters:

- 1. learning rate (lr) = 1e-3
- 2. steering layer (L) = 10
- 3. steering strength (α) = 4
- 4. number of epoch (e) = 3

P.1 PCA Activations Across Experts

Layer 2



Figure 17: PCA Activation Across Experts at Layer 2 of OLMoE Model

Layer 8



Figure 18: PCA Activation Across Experts at Layer 8 of OLMoE Model

Layer 14



Figure 19: PCA Activation Across Experts at Layer 14 of OLMoE Model

Q Computational Requirements

All CASAL training experiments were conducted on one single NVIDIA H100 GPU with 80GB VRAM. Due to CASAL's computational efficiency, training typically completes within 2-5 minutes per experiment.

R The Use of Large Language Models

Large language models (specifically GPT5, Claude Sonnet 4, Gemini 2.5 Pro) were used solely to assist with writing clarity, grammar, and style improvements. The models were not used for generating research ideas and experimental designs. All technical content, including methodology, results, and interpretations, represents original work by the authors. Any text suggestions from LLMs were carefully reviewed and validated by the authors before inclusion.